UNIVERSITÀ DEGLI STUDI DI PADOVA

DIPARTIMENTO DI INGEGNERIA DELL'INFORMAZIONE

DIPARTIMENTO DI INGEGNERIA DELL'INFORMAZIONE

CORSO DI LAUREA MAGISTRALE IN BIOINGEGNERIA

"Neurofeedback BCI based on complexity of the EEG signal for treatment of cognitive disorders"

Relatore: Prof. Stefano Tortora

Laureando: Federico Nordio

ANNO ACCADEMICO 2023 - 2024

Data di laurea 02/12/2024

Contents

1. **Introduction**
   1.1 Overview of cognitive disorders
   1.2 Causes, effects and treatments of cognitive disorders
   1.3 Brainwaves and frequency bands
   1.4 Neurofeedback
      1.4.1 Closed loop
      1.4.2 Electrode placement
      1.4.3 Recording brain activity
      1.4.4 Online data processing
      1.4.5 Feature extraction and complexity measures
      1.4.6 Feedback generation and types
      1.4.7 Learning and brain plasticity
   1.5 Neurofeedback issues and future challenges
   1.6 Objectives
2. **Materials and Methods**
   2.1 System Overview
   2.2 EEG cap
   2.3 ROS and ROS-Neuro
   2.4 Processing
      2.4.1 Laplacian filtering
      2.4.2 PSD, Welch method and 1/f trend
   2.5 Complexity measures
      2.5.1 Spectral Entropy
      2.5.2 Spectral Asymmetry Index
      2.5.3 Relative Power
      2.5.4 Band Power Ratios
      2.5.5 Power Law Exponent
   2.6 Coloured noise
      2.6.1 White noise
      2.6.2 Pink noise
      2.6.3 Brown noise
   2.7 Nodes
      2.7.1 Acquisition node
      2.7.2 Laplacian node

2.7.3 PSD node

2.7.4 PLE computation node

2.7.5 PLE to noise node

3. Experiments and Offline analysis

3.1 Experimental protocol

3.2 Offline Analysis

4. Results and Discussion

4.1 PLE raw and smoothed

4.2 PLE for unfiltered and filtered signals

4.3 Correlation between EOG and unfiltered and filtered EEG signals

4.4 Correlation between PLE in CZ and PLE of all adjacent channels

4.5 Comparison between complexity metrics and PLE

4.5.1 Spectral Entropy

4.5.2 Spectral Asymmetry Index

4.5.3 Relative Power

4.5.4 Band Power Ratios

4.5.5 Correlation between PLE and complexity measures

4.6 Linear trend

4.7 Topographic maps

4.8 Sound generation

4.9 Mean and Standard Deviation before and after filtering

5. Conclusions

6. Bibliography

Chapter 1. Introduction

1.1 Overview of cognitive disorders

Cognitive disorders represent a complex category of conditions that impair an individual's ability to carry out normal brain functions. These impairments can affect various aspects including memory, attention, problem solving, learning and communication with the outside world (Fig. 1.1).

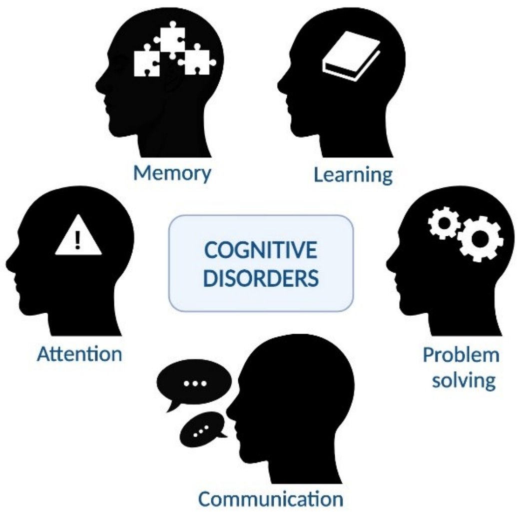

Fig.1.1: Schematic representation of cognitive functions affected by cognitive disorders.

Cognitive disorders are studied across multiple disciplines, such as neurology, psychology, psychiatry, and engineering, as they have a significant impact on both the affected individuals and those around them. They are not limited to a specific age group but concern the entire population. Patients with these problems often experience a reduced quality of life, with a loss of autonomy in performing daily activities, difficulties in intrapersonal and interpersonal relationships, and a need for continuous support from caregivers even for the simplest tasks. This leads to an increase in health costs, a loss of productivity as well as a difficulty for families to take care of these subjects. In the field of engineering, special attention is given to identify the most accurate indicators that can describe individual's cognitive state. In recent years, research in this area has introduced various indices to monitor performance and provide an objective clinical picture. The research has moved on to the frequency analysis of electroencephalographic activity and in particular to the spectrum of the electroencephalographic (EEG) signal [1]. The main studies were conducted in subjects with Alzheimer's disease (AD), subjective cognitive decline (SCD), mild cognitive impairment

(MCI), attention deficit hyperactivity disorder (ADHD) and locked-in syndrome (LIS). SCD refers to the phenomenon of the subject's preoccupation with having cognitive dysfunction despite the fact that the markers do not highlight abnormalities. Cognitive tests do not show significant impairments, but the subject perceives a worsening of memory or other cognitive functions. Even if it does not emerge from cognitive tests, it is important to monitor the health of the subject as he is more likely to develop more significant cognitive deficits such as MCI or AD [2]. MCI is defined as a condition in which individuals exhibit obvious cognitive problems that affect memory, thinking, and reasoning ability but who do not meet the criteria for dementia. The changes in this pathology are more pronounced than those expected with aging but do not significantly interfere with normal cognitive decline. Often this condition represents the phase prior to Alzheimer's disease or other dementias [3, 4, 5, 6]. AD is a progressive neurodegenerative disorder that predominantly affects memory, thinking, and behaviour. It is the most prevalent cause of dementia and leads to a gradual decline in cognitive abilities. The disease arises slowly and worsens over time, leading to a loss of autonomy of the affected person. Amyloid plaques are created in the brain that disrupt cellular communication and neurofibrillary tangles that lead to the degradation of the internal structure of neurons. These phenomena lead to the atrophy of the areas involved in memory and reasoning tasks [3, 6, 7, 8, 9]. ADHD is a neurological disorder characterized by continuous patterns of inattention, hyperactivity, and impulsivity that interfere with cognitive functioning or development. The causes that lead to the manifestation of ADHD are of different types: genetic factors, brain structural factors, environmental factors such as exposure to lead or childhood trauma. There are three different subtypes of ADHD. Predominantly inattentive presentation, also referred to as attention deficit disorder (ADD), is a form in which the main symptom is inattention and manifests itself as difficulty concentrating and organizing. Overactive or impulsive presentation may include constant restlessness and difficulty controlling impulses. Finally, combined presentation is the most common form of ADHD and has both aforementioned issues [10, 11, 12, 13, 14, 15, 16]. LIS is a neurological condition in which the individuals are aware of what is happening around them but, due to issues related to muscle movement, are unable to communicate or interact with their surroundings. This state occurs following damage to the brainstem, strokes, or other neurological conditions that, however, still allow the person to retain cognitive functions such as seeing, hearing, thinking, and remembering. There are several stages of LIS. Classic LIS is the most common type, and the patient is only able to perform eye movements, allowing communication through this single channel. In the incomplete variant of LIS, individuals have a certain degree of voluntary movement, such as in the fingers or toes, enabling better communication compared to classic LIS, although eye movement remains the primary communication method. Finally, complete LIS (CLIS) is the most severe form of LIS, in which all movement abilities, including eye movements, are lost. Communication is very challenging, but attempts are being made to establish direct communication with the individual through the use of Brain-Computer Interfaces (BCIs). It has been hypothesized that a progressive reduction or extinction of goal-directed thinking could be the cause of the cessation of voluntary cognitive activity. In some cases, no communication is possible because not all individuals are able to use this type of technology [17, 18, 19, 20].

1.2 Causes, effects, and treatments of cognitive disorders

Cognitive disorders can arise from various causes, including traumatic brain injuries, the prolonged use of certain pharmacological substances, chronic infections that affect specific brain regions, and psychiatric conditions that manifest early in life or remain latent for years before emerging in older age. These causes can lead to disorders of high functions such as general intelligence, attention, memory, judgment, inhibition, cognitive flexibility, planning, language, visual and spatial skills [21]. Diagnosing cognitive disorders is challenging, as they can present in different forms and vary subtly over time in both intensity and manifestation. Some of these disorders have no cure, but some treatments are available that allow the progression of the disease to be slowed down. Advances in different areas of study have improved understanding of disorders, but treatments and cures remain limited. The current treatments for cognitive disorders include:

- Medications: antidepressants, inhibitors, memantine, stimulants, and antipsychotics.
- Cognitive rehabilitation: structured exercises and compensatory strategies aim to improve specific cognitive tasks.
- Behavioural and psychosocial interventions: targeting the psychological and social aspects of cognitive disorders.
- Lifestyle interventions: exercise, diet management and sleep organization that have shown benefits in managing symptoms.
- Assistive technologies: virtual reality applications and communication devices to support cognitive tasks, especially for individuals with language deficits.
- Emerging therapies: transcranial magnetic stimulation (TMS), stem cell therapies, gene therapies, BCIs, and Neurofeedback (NFB) are gaining attention for their potential in treating cognitive disorders.

However, these treatments often have side effects. Pharmacological treatments may cause bradycardia, muscle cramps, gastrointestinal issues, confusion, insomnia, anxiety and agitation. Non-pharmacological approaches, such as cognitive rehabilitation, physical exercise and psychosocial interventions, on the other hand, can lead to problems like mental fatigue, frustration, anxiety and injuries. For the approaches with assistive technologies, may result in dependency, and neurostimulation techniques can sometimes cause headaches or seizures. Stem cell therapy, though promising, carries risks of tumour formation and immune rejection. As can be seen, in addition to bringing improvements to the psychophysical state of the individual suffering from cognitive disorders, the various therapies have side effects that impact its life. This fact underscores the need for continuous research and the development of new therapeutic approaches to better manage cognitive disorders and improve patients' quality of life. Recent advancements in treatment approaches include the use of BCIs and NFB [22]. BCIs are systems that exploit brain signals, which are processed and used to control external devices such as exoskeletons, robotic arms or motorized wheelchairs allowing neuromuscular pathways to be bypassed. NFB, on the other hand, monitors brain activity in real-time, providing feedback to the user that allows him to learn how to modulate brain activity itself. While BCI is considered a two-way method, since the machine and the subject learn from each other, NFB is a one-way method, as it is the subject who adapts to the machine. Both techniques control brain activity through a closed-loop system, and both can induce plasticity in the subject who learns to modulate brain waves [22]. Brain plasticity is a fundamental concept in neuroscience, and it refers to the ability of neural networks to reorganize their structure and to modify their functions in response to intrinsic or extrinsic stimuli [23]. Other similarities shared by the two techniques concern the signals acquisition (which usually takes place through the use of EEG), the real-time processing (to provide immediate feedback or control), and the processes of learning and adaptation accomplished by the subject, (which can take place both to control a device, and to modulate brain rhythms activity). NFB can be used for three main purposes [19, 24]:

1. Therapeutic: it can be used as a therapeutic tool to reduce symptoms in conditions such as motor impairments, ADHD, epilepsy, or recovery after stroke [10].
2. Performance enhancement: boosting cognitive abilities in healthy subjects through peak performance training. [21, 25]
3. Experimental research: exploring the causal role of specific neural events on cognition and behaviour through brain-state-dependent stimulation (BSDS) [24].

1.3 Brainwaves and frequency bands

Both NFB and BCI technologies rely on monitoring and modulating specific brain wave patterns to achieve therapeutic effects [22]. Brain oscillations are the rhythmic electrical activity generated by neural tissue that can be spontaneous or in response to stimuli. Oscillations in the Alpha, Beta, Gamma, Delta and Theta frequency bands are altered throughout the cortex in pathological subjects and especially in subjects with cognitive impairment. [13] The recording of brain waves is able to capture patterns recognizable by the amplitude and frequencies of the waves. Amplitude represents the power of brain waves. It reflects the degree of synchronization of neurons, and greater synchronization implies a greater amplitude of the signal. EEG signals range in amplitude from 10 to 200 microvolts (μV). Frequency indicates the number of oscillations in a time interval and is measured in Hertz (Hz), which is the number of cycles per second. The main frequency bands are in the range 0,5-40 Hertz (Hz) (Figure 1.1).

- Delta waves (0.5-4 Hz): Delta waves are associated with deep sleep and unconsciousness. Abnormal activity of these waves in awake adults could mean brain trauma, cancer or other neurological disorders. These waves are usually observed in the frontal region during sleep but can arise globally throughout the brain [13].
- Theta waves (4-8 Hz): Theta waves are linked to light sleep, relaxation, and meditative states. They are often increased during creative activities, memory processing, and certain cognitive tasks. Elevated Theta levels may be associated with conditions like ADHD, emotional stress [26], or other cognitive disorders. These waves commonly originate in the hippocampus and temporal lobes, though they can also appear in other regions during relaxation [5, 13, 27].
- Alpha waves (8-13 Hz): Alpha waves are associated with relaxed, wakeful states, particularly when the eyes are closed, and sensory input is minimal. Alpha activity is dominant in spectral analysis and decreases during activities requiring focused attention or cognitive effort. These waves are primarily observed in the occipital, parietal, and frontal regions of the brain [5, 13, 27, 28].
- Beta waves (13-30 Hz): Beta waves correspond to active thinking, attention, problem-solving, and mental effort, and are prominent during alert and concentrated states. High Beta activity is linked to stress [26] and anxiety, whereas lower Beta activity may indicate attention deficits. The frontal region shows the most significant Beta wave activity.
- Gamma waves (>30 Hz): Gamma waves are associated with high-level cognitive functions like perception, problem-solving, memory, learning, and sensory processing. They play a crucial role in creating unified perceptions across different sensory inputs. Abnormal

Gamma activity has been linked to cognitive dysfunctions and certain mental health conditions, including schizophrenia [13].

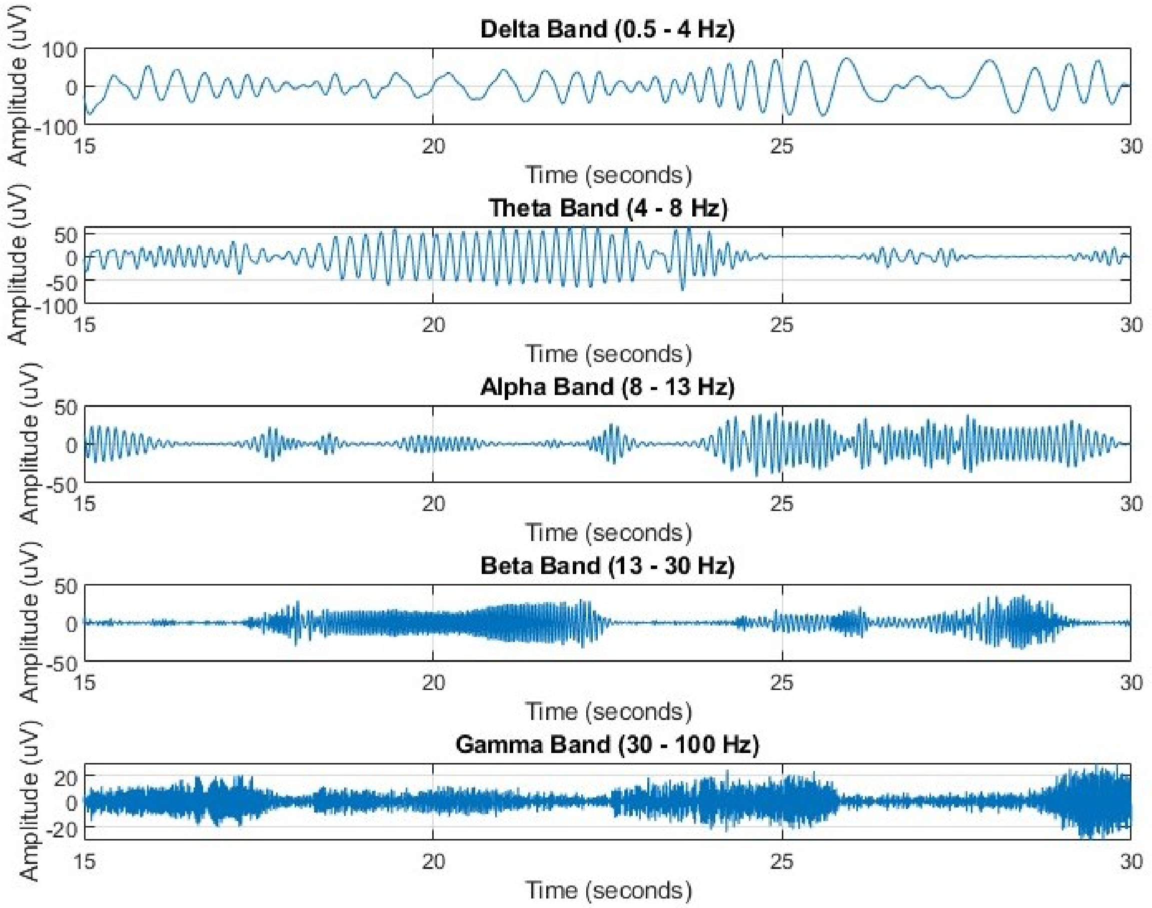

Fig. 1.2: This image represents the main frequency bands that constitute an EEG signal, created through digital synthesis. The EEG signal was generated by combining the Delta, Theta, Alpha, Beta, and Gamma rhythms, modelled as sinusoidal signals at specific frequencies with varying amplitudes, based on values from the literature to closely resemble real EEG data. Gaussian background noise was added to mimic real-world conditions. To simulate time-varying amplitudes, modulation was applied to the amplitudes across the different frequency bands. Additionally, causal spikes were introduced to represent artifacts such as muscle or eye movements. To extract the individual frequency bands, 4th-order digital Butterworth bandpass filters were applied to the synthesized EEG signal. This image was created using MATLAB.

The study of the EEG signal strength allows for the detection of structural and physiological changes in brain status. For example, through the analysis of the Theta and Alpha band in subjects with AD, a correlation with subcortical changes has been highlighted. Specifically, an increase in Theta band power and a decrease in Alpha band indicate hypoperfusion (i.e. an inadequate blood supply to the brain), which can lead to brain tissue death. In addition, it is shown that in subjects with AD the activity related to the Theta band is higher and the activity in the Beta and Alpha bands in a resting state is lower, indicating a general slowdown in activity. In patients with MCI, findings regarding Alpha band ratios have been reported. By calculating the ratio between the upper and lower Alpha bands, researchers have noted that a higher ratio correlates with temporo-parietal cortical thinning, hippocampal atrophy, and reduced cerebral perfusion in the medial temporal cortex [28]. An increase in Theta band activity has also been observed in these patients. Many studies performed on ADHD patients find an increase in Theta activity and therefore an overall slowdown in brain activities especially in the frontal and central regions that are responsible for attention, impulse control and executive functions. The increase in Theta waves is associated with reduced concentration and poor brain activation. In addition to the increase in Theta band power, there is also a reduction in Beta band activity in the frontal regions [29]. The most documented finding in ADHD during the EEG study is the increase in the ratio of Theta band power to Beta band power [15]. This increase reflects increased inattention and reduced cognitive control. Studies on Alpha activity have also been conducted but have not led to stable conclusions on the use of these frequencies for diagnosis or for training subjects. However, it is highlighted that variations in this band could signal malfunctions in the excitation and relaxation mechanisms [19, 21 30, 31, 32].

1.4 Neurofeedback

1.4.1 Closed loop

NFB is a type of biofeedback that the subject uses to train himself to control and improve his brain functions [24]. This feedback is produced proportionally to the subject's brain activity by monitoring, through special devices, the waves produced by the brain. This technique may or may not include using direct stimuli or tasks for training. After the neural information is sent to a processing software, the outgoing data is sent to the brain creating a loop. This allows the brain to modulate its activity through auditory, visual, electrical, magnetic or tactile stimuli. The applications of NFB differ in the type of waves used, electrode positioning, electrode mounting, types of protocols, signal processing, integration of other techniques and type of software used [11, 25, 33]. The diagram depicting the main steps of the NFB is represented in Fig. 1.3.

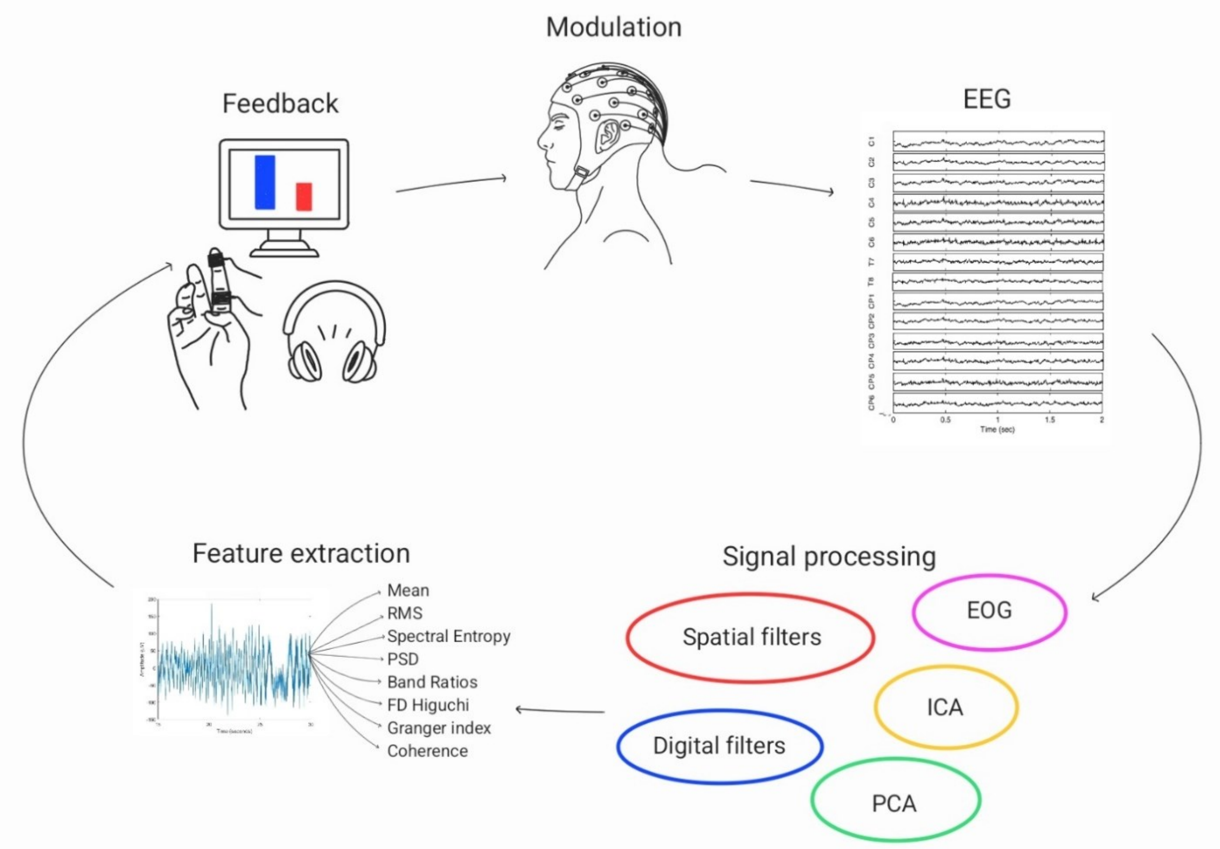

Fig. 1.3: Diagram representative of the closed loop of the NFB.

1.4.2 Electrode placement

The first step in the NFB procedure is the placement of electrodes on the subject's scalp. Electrodes are employed for EEG, which is the most widespread technique for measuring the electrical activity of the brain. The electrodes used for EEG measurements can be of three types: adhesive scalp electrodes, hypodermic needle electrodes (inserted under the skin), and electrodes fixed on a cap. The signal display can be set through different montages. In the reference montage, each waveform represents the voltage difference between an active electrode and a reference electrode. There is no standard location for the reference electrode, but it is usually placed in a region with minimal brain activity. In bipolar montage, each waveform represents the voltage difference between two adjacent electrodes. In the average reference montage, the activity of all electrodes is averaged and used as a reference. Finally, in Laplacian montage, the reference for each electrode is a weighted average of the surrounding electrodes. The placement of the electrodes on the scalp is crucial for the extraction of meaningful signals. For this reason, standards that divide the skull in different areas have been introduced to permit the comparison of intra- and inter-subject signals [13]. The best-known placement system is the 10-20 standard (Fig. 1.4).

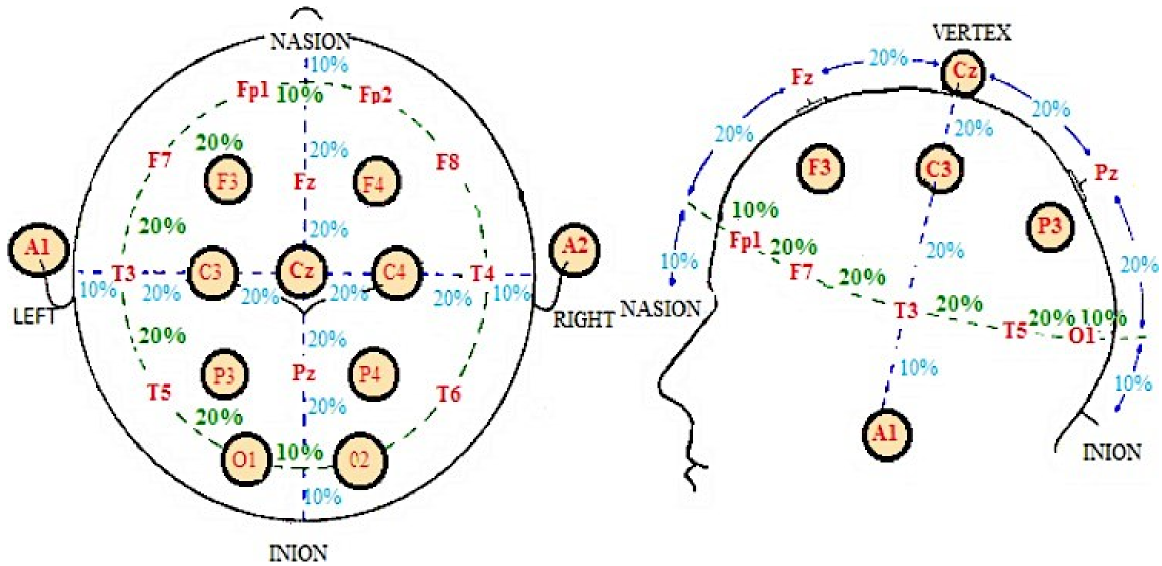

Fig. 1.4: Representation of the 10-20 standard [13].

In this standard, the placement of the electrodes takes place at intervals of 10% or 20% of the total distance between specific positions of the skull which are the Nasion (small depression in which nasal and frontal bones meet), the Inion (bony prominence located at the back of the skull), and the preauricular points (bony landmarks located on either side of the head, just in front of the earlobes). This standard ensures that the electrodes are positioned according to the size of the head ensuring consistent placement across different subjects. The different regions of the skull are identified by letters. The letters F, P, T, O and C refers to frontal, parietal, temporal, occipital and central areas respectively. Odd and even numbers identify the left and right side of the skull, respectively. The numbers are replaced by the letter Z in the centreline. Fp1 and Fp2 are the left and right poles of the forehead respectively, A1 and A2 refer, respectively, to the left and right sites near the ears, which are common sites for the reference electrode [13]. The montages predominantly used during NFB are unipolar and bipolar. In the case of unipolar mounting, the activity of the electrode under consideration is compared with a reference electrode which ideally does not register any electrical activity and is therefore positioned far from sources of brain activity. In the bipolar mode, on the other hand, signals from two electrodes positioned on the skull are used. The advantage of this mode is common-mode rejection; in fact, common activities that are in the two channels are deleted. Each brain area represents specific functions and tasks, and the study of specific areas can provide specific information about the subject's behaviour. The traditional division of the brain into lobes is illustrated in Fig. 1.5.

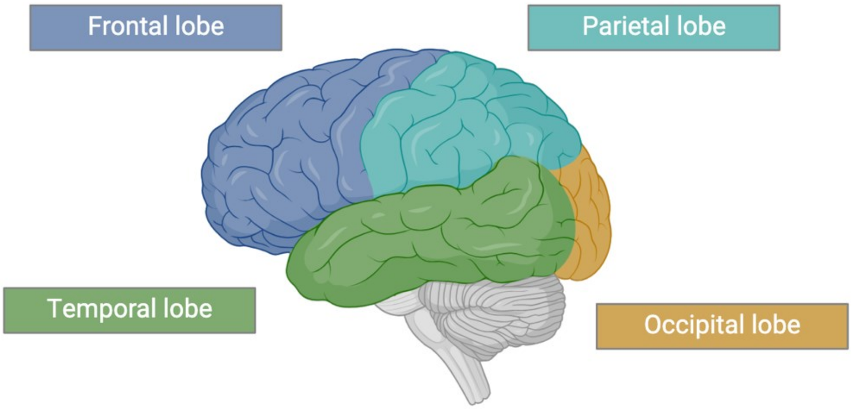

Fig. 1.5: Representation of brain lobes.

The parietal lobes are involved in the functions inherent in problem solving, lexical formulation, attention, performing mathematical calculations, spatial and geometric association. A disorder in these areas could lead to dyscalculia, problems with orientation and learning disorders. The frontal lobes are responsible for concentration, planning, and positive emotions. Impairments in these regions can result in depression, anxiety, fear, and poor executive functioning. The temporal lobes play a crucial role in auditory processing, language comprehension, visual learning and reading, and an eventual malfunction of these can lead to learning disorders, auditory disturbances and personality changes. The occipital lobe is primarily involved in visual processing, and it plays a key role in spatial orientation and visual memory. A damage in that area could lead to vision loss or problems with orientation. For studies involving the use of NFB, the main areas taken into consideration are the sensorimotor cortex and the cingulate gyrus (Fig. 1.6).

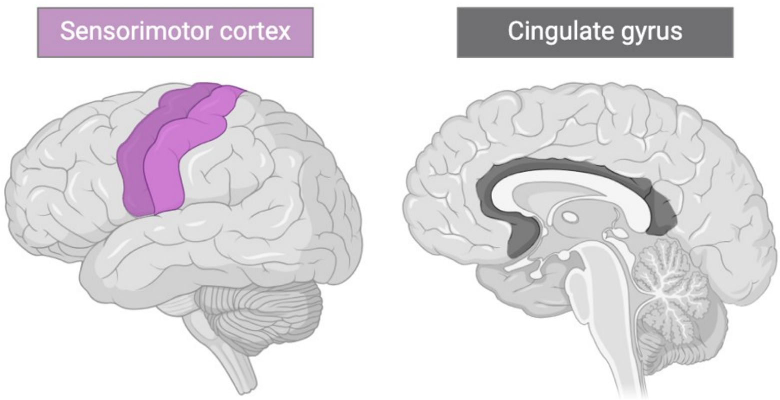

Fig. 1.6: Representation of sensorimotor cortex from lateral view and cingulate gyrus from sagittal cut view.

The sensorimotor cortex is essential for attention, mental processing, fine motor activities, sensory and motor processing and manages emotions, calmness and empathy. A disorder or trauma in this area can lead to paralysis, seizure disorders, and ADHD symptoms. The cingulate gyrus is responsible for mental flexibility, attention motivation and morale and trauma in this area could result in tics, worry, ADHD and OCD (obsessive compulsive disorder) [33]. The Boca area is involved in verbal expression, and its impairment can lead to dyslexia and other reading and writing disorders. The electrodes that cover these regions, important in NFB applications, are CZ, C3, C4, Fpz, Fz, Pz and Oz [13].

1.4.3 Recording Brain Activity

The second step is the measurement of brain activity which takes place through EEG using electrodes placed on the subject's scalp. What is measured by EEG is the neuronal activation that provides us information about the general activity of a certain area of the brain. EEG is the recording of the synchronous activity of neurons of the area, in particular, of pyramidal neurons that are arranged perpendicular to the skull [1, 22]. EEG is a non-invasive technique that involves placing electrodes on the scalp to measure fluctuations in electrical potentials. EEG, like other brainwave recording techniques, offers pros and cons in its application. The main advantage, for which EEG is preferred as a method of recording, is the high temporal resolution. Brain activity is recorded in milliseconds (ms), allowing wave changes to be captured in real time. A high time resolution is essential in online applications. Another advantage is the non-invasiveness that allows to not intervene on the patient with the grafting of electrodes under the skin or in the brain itself as happens in other invasive techniques. One of the disadvantages is the low spatial resolution, since only the activity of populations of surface layer neurons is recorded and this leads to the loss of information of what is happening in the deepest areas of the brain. Another disadvantage is the sensitivity to noise and artifacts. An artifact is an electrical activity that does not come from the brain. There are two types of artifacts: physiological and extra-physiological. Physiological artifacts are generated by the subject and derive from sources other than the brain and can be eye movement, electrocardiographic activity, sweat, muscle activity. Extra physiological artifacts derive from outside the body and can include poor contact between skin and electrode, bad contact between electrode and cable, electromagnetic interference, environmental or instrumental artifacts, the power supply of the device (which, depending on the device, introduces a frequency component at 50 or 60 Hz). However, through filtering and signal processing techniques it is possible to reduce the impact of artifacts on the signal. There are other techniques for measuring brain signals such as magnetoencephalography (MEG), functional magnetic resonance imaging (fMRI), positron emission tomography (PET) and near-infrared spectroscopy (NIRS), but given the advantages that EEG brings to NFB, this technique is preferred over those previously mentioned [11, 33, 34].

1.4.4 Online data processing

The third step is to process the data online. This phase involves several steps that allow to convert a raw signal into a clean one. The processed signal will then be used for the extraction of the features. Generally, the signal is filtered to remove the sources of noise and artifacts present in it. Noise and artifacts sources can be different, and each of them has a different approach for its elimination. The most frequent applied techniques are analogical and digital filters. Analogical filters, used in the preprocessing phase, are exploited to have a general and not too aggressive filtering of the signal through electronic circuits including resistors, capacitors and inductors. Subsequently, the signal is digitized through the use of an Analog to Digital Converter (ADC), and it is filtered through digital filters which, on the other hand, allow certain frequency bands to be eliminated or kept through the use of algorithms and calculations. There are different types of filters and applications of them. The most well-known are low-pass, high-pass, and band-pass filters. Low-pass filters allow to maintain frequency amplitudes that are lower than a user-chosen cutoff frequency, high-pass filters ensure that frequencies greater than a certain frequency are maintained, and bandpass filters maintain a range of signal frequencies. These filters can have different order which is determined by the complexity of the filter itself. The applications of these filters can be motivated by the removal of noise at low or high frequencies or to facilitate the passage of certain frequency bands. The more complex the filter is, the higher the order of the filter. More complex filters allow to obtain better filters at the expense of greater computational complexity. Another filter widely implemented in this phase is the Notch filter. It is commonly used for the elimination of interference usually due to the mains power supply which, in electronic equipment, is at a frequency of 50 Hz or 60 Hz. Notch filter allows the frequency components around a central frequency to be strongly attenuated, leaving the other components unaltered. Another type of filtering is the spatial filtering that is useful for improving signal quality by isolating relevant neural activity. This type of filtering involves the implementation of linear operations using weights associated with different channels. Eye movement artifact may occur during EEG recording. This artifact introduces unwanted variations within the recorded track that compromise the real trend of the signal. These are waves that do not have a specific frequency band to eliminate since blinking is a random movement and therefore filtering in the frequency domain cannot be applied in this case. An electrode is then placed under the eye that records the activity in that area at the same time as the other electrodes, placed on the scalp, record the brain activity. This electrode allows to detect the grade of closing and opening of the eyelids and therefore to determine the extent of the artifact. Filtering by regression is widely used and the goal is to model the relationship between the artifact and the EEG signals. When the relationship between these is established, the artifact is subtracted from the signal. The most widely used model is the linear regression model because it is computationally fast and therefore applicable online. The model assumes that each signal from each channel is a linear combination of the true signal and the contribution of the artifact measured by the electrooculogram (EOG). Regression coefficients, which represent the contribution of EOG within the EEG signal, are then estimated using the linear regression model using different optimization techniques. Subsequently, having the regression coefficients, the contribution of the EOG is calculated and it is subtracted from the raw EEG signal to obtain the clean EEG signal. However, the assumption of linearity between signals may be invalid and therefore lead to inaccurate results. Another problem is bidirectional contamination, i.e. the recording of the EOG can include traces of neural potential and therefore the removal of the signal deriving from the EOG electrode could also eliminate information on brain activity [34]. To avoid these limitations, more efficient algorithms are introduced. Among the noise and artifact reduction algorithms there is the principal component analysis (PCA). This technique allows to identify the principal components that represent the greatest variance of the signal. Since the contribution of noise and artifacts to the signal variance is very small, it will be enough to keep the main components and, with these, reconstruct the EEG signal obtaining a clean signal. Another technique is the independent component analysis (ICA) which separates a multivariate signal into its additive subcomponents under the assumption that they are non-Gaussian signals statistically independent from each other. These techniques bring improvements in the quality of the filtered signal but are computationally expensive and therefore not used in real-time applications [34, 37].

1.4.5 Feature extraction and complexity measurements

Once the signal has been filtered, the next step is the extraction of significant features. This is a fundamental phase because the type of features extracted indicates a specific pattern of the analysed signal. The features can derive from time, frequency, and time-frequency domains analyses [34]. In recent years, particular attention has been given to features that describe the complexity and distribution of EEG signals for NFB applications in the context of cognitive disorders. The most commonly used time-domain features are mean, variance, skewness, kurtosis, Root Mean Square (RMS), and peak-to-peak amplitude of the signal. In the frequency domain, the Power Spectral Density (PSD) is used to describe signal power within specific frequency bands [18, 20, 26]. This metric is used to track the activation or deactivation of specific brain frequencies. The spectral entropy measures the complexity of the PSD. High values of spectral entropy indicate an unevenly distributed spectrum, suggesting greater complexity. This index helps to identify changes in brain activity patterns, such as transitions between different states or effects of neurological disorders. Other indices are the power band ratios. They provide insights into the cognitive states of the subject. In fact, by comparing the power across different bands, it is possible to extract information on the dominance of specific frequencies over others, indicating particular mental or physiological states. The most well-known time-frequency features are Wavelet coefficients, which describe information on time-varying frequencies. The Wavelet transform analyses non-stationary signals, like EEG. It uses inner products to measure the similarity between a signal and a function called the Mother Wavelet, allowing for the analysis of induced activity and characterization of responses to specific events [34]. The Hilbert transform allows for the extraction of the instantaneous amplitude, which reflects the power brain rhythm, the instantaneous phase, for the study of phase synchronization between different areas, and the instantaneous frequency, that allows to track the dynamic changes of oscillations at various frequencies, from non-linear and non-stationary signals [4]. In addition, this transform enables to study the changes in different frequency bands over time through time-frequency analysis by. Event-related spectral perturbation (ERSP) measures event-related changes in the power spectrum by providing information on the change in oscillatory activity of the brain and how different frequency bands vary during cognitive processes. There are also non-linear features based on complexity, which are useful for classifying brain states and detecting anomalies [34]. Among these, the concept of fractal size is used, such as the Higuchi fractal dimension, which measures the complexity of the signal by reflecting its self-similarity at different scales. Approximate Entropy (ApEn) and Sample Entropy (SampEn) are also used to measure signal predictability; in these metric, lower values indicate greater regularity, and higher values indicate more irregularity and complexity. The Sample Entropy is more robust to noise and short time series. Connectivity-based features can be extracted, to capture interactions and dependencies between different brain regions. Functional connectivity tries to pinpoint whether neural activity between two regions is related. In this type of connectivity, the directionality of the interaction is not investigated but only its existence [1, 9]. Effective connectivity, on the other hand, measures the causal relationship between two areas. Coherence index measures synchronization between two signals in the frequency domain, high values of it indicate functional connectivity between two regions at a particular frequency [4]. Granger causality is another parameter used to measure effective, or directional, connectivity, indicating whether one EEG signal can predict another, by suggesting causal relationships between different brain regions. In literature, many complexity measures are cited to describe brain dynamics and investigate subject health. Many of these measures, however, have a high computational time, making them unsuitable for online applications [1, 10, 33].

1.4.6 Feedback generation and types

Depending on the disorder and the needs of the subject, different types of NFB can be employed, characterized by the way in which the feedback id delivered, which can be visual, auditory or tactile [13]. The choice of feedback modality significantly influences individuals' ability to regulate brain activity. The most common and frequently used modality is the visual sensory one, which involves presenting the subject with images, animations, or graphs that change in response to brain activity. For example, a bar graph could represent the amplitude of different brain wave frequency bands, and through training, the subject should try to bring the band amplitudes back to physiological levels. Other techniques include the use of video games or augmented virtual reality that allow the subject to move or progress in virtual environments through the modulation of their brain waves [22]. This system is widely used in individuals with ADHD. Tactile, or haptic, feedback uses physical sensations to inform the subject of their brain activity. This is one of the least used techniques but is often used in subjects with poor visual or auditory processing capabilities. This feedback is delivered via pressure, temperature changes, or vibrations on the skin. For example, in a vibrational NFB, if the individual's waves are within physiological ranges, a vibration is delivered. As long as the subject remains in the physiological ranges, the vibrations will continue to provide a form of reinforcement through physical sensation. Auditory feedback uses sounds to provide real-time information about brain activity. The brain's electrical activity is translated into sound frequencies or musical tones that vary in pitch, volume, or frequency. Among its various applications, there is the treatment of individuals with high levels of stress and anxiety, where the goal is to increase Alpha waves often associated with calm states. Treatments for individuals with ADHD [28, 33], instead, involve the use of sound signals that vary according to the individual's state of attention. In these cases, Beta waves are monitored and modulated to fall within physiological ranges. The main advantage of using auditory NFB is the accessibility of the treatment; this technique allows individuals with visual or sensory disabilities to benefit from it. Other benefits include less distraction, integration into daily activities, and deep immersion in states of relaxation that improve the effectiveness of the treatment. In several studies, the effect of auditory stimulus has been compared with visual stimulus. The auditory stimulus takes about 8 to 10 ms to reach the brain while the visual stimulus takes 20 to 40 ms and for this reason the auditory effect is greater than the visual one [38].

1.4.7 Learning and brain plasticity

External stimuli can cause behavioural responses throughout the body. When the feedback signal is delivered to the subject, the phase of signal processing and brainwave modulation occurs. Feedback implies that brain outputs cause, through a system, the brain inputs themselves. NFB learning can be conceptually represented through closed-loop models based on control theory. In fact, initially the signal reflects a random neural variability and therefore the activity will not generate enough activity to reach the thresholds for reward. After the presentation of the sensory feedback signal, the brain releases a signal modulated by the reward, and from this point onward, the closed-loop cycle begins, in which the subject has to modulate his own activity to obtain more and more positive responses from himself. Brain plasticity, or neuroplasticity, is a characteristic that allows the brain to adapt and change by reorganizing and forming new neural connections in response to learning. It is a fundamental quality for memorization, cognitive development and recovery from injuries. The mechanisms underlying neuroplasticity, such as synaptic plasticity, neurogenesis, and cortical remapping, allow the brain to create new connections and rearrange itself in response to experience. Synaptic plasticity involves changes in the strength of connections between individual neurons, while structural plasticity entails reorganization of neural networks and, thus, cortical remapping. Hebb’s principle states that "when an axon of one neuron is close enough to repeatedly and persistently excite another neuron, metabolic changes and growth processes occur in one or both neurons, enhancing their efficiency" [10, 22, 25]. This suggests a strengthening of connections in response to an external reward stimulus. By providing real-time feedback on brain activity, NFB taps into the brain’s plastic potential to promote lasting cognitive and behavioural improvements. Changes in neural connections become more deeply rooted, leading to lasting improvements in cognitive and emotional regulation [10, 22, 23, 33].

1.5 Neurofeedback issues and future challenges

Neurofeedback (NFB) therapy has already been tested for some conditions, showing potential in modulating specific electrophysiological activity for several disorders, like ADHD, epilepsy, autism spectrum disorder, traumatic brain injury, depression, and anxiety. Despite the numerous scientific evidences, many studies do not demonstrate the therapy effectiveness or are limited by factors such as the number of subjects, the number of training sessions, the number and placement of the electrodes, the feedback timing, the type of reward, and the types of extracted features. The absence of standard protocols and guidelines is a significant problem when attempting to draw conclusions across diverse populations. These issues contribute to the insufficient evidence for NFB to draw firm conclusions about its efficacy. Another challenge noted in this field is the standardization of therapy across large pool of subjects. Some individuals are unable to learn to modulate brain activity effectively. In fact, it is observed that there are people who are not able to learn to modulate brain activity. This problem arises in a higher percentage in the experiments in which the same protocol is used for all subjects, while the percentage of non-responders decreases when the protocols are personalized. NFB training can also lead to adverse responses that temporarily increase symptoms commonly associated with central nervous system relaxation, such as fatigue, headaches, dizziness, mood swings, insomnia, anxiety, and difficulty concentrating. All these reactions are generally temporary, making NFB a low-risk therapy [10, 13, 24, 34].

1.6 Objectives

The aim of this thesis is to create an innovative model of closed-loop passive auditory NFB. From recent studies it has been seen that the EEG activity in frequency domain follows the coloured noise trend [20, 22, 35, 36]. The idea is to build a system that allows to generate a sound proportional to the brain activity of the subject exploiting the complexity of the EEG signal. To do this, it is necessary to investigate the nature of the EEG signal and its dynamics, paying more attention to the brain activities of healthy subjects and those with cognitive disorders. For the creation of the auditory feedback, several aspects of signal processing need to be considered. To do this, a preliminary phase of offline testing is implemented to investigate the effects that filtering has on the signal and which are the appropriate complexity metrics to capture its dynamics. After taking the necessary considerations on the NFB specifications and identifying the most descriptive complexity metric of the signal spectrum, the code for real-time processing is implemented. The first experiments are then carried out, recording the electrical brain activities of some healthy subjects during the administration of auditory feedback. The signals collected are then processed and analysed in a final offline phase that allows conclusions to be drawn on the effectiveness of the proposed NFB. In this phase, the recorded signals are compared between the NFB implemented in real-time and the signals from a more complex offline processing of the signals.

Chapter 2: Materials and Methods

2.1 System Overview

The NFB system that has been built up presents an auditory feedback able to track the brain activity of the subject. To realize this process, it was necessary to implement a closed loop that from the recording of the EEG signal produces an output sound proportional to the current measure of complexity of the brain activity.

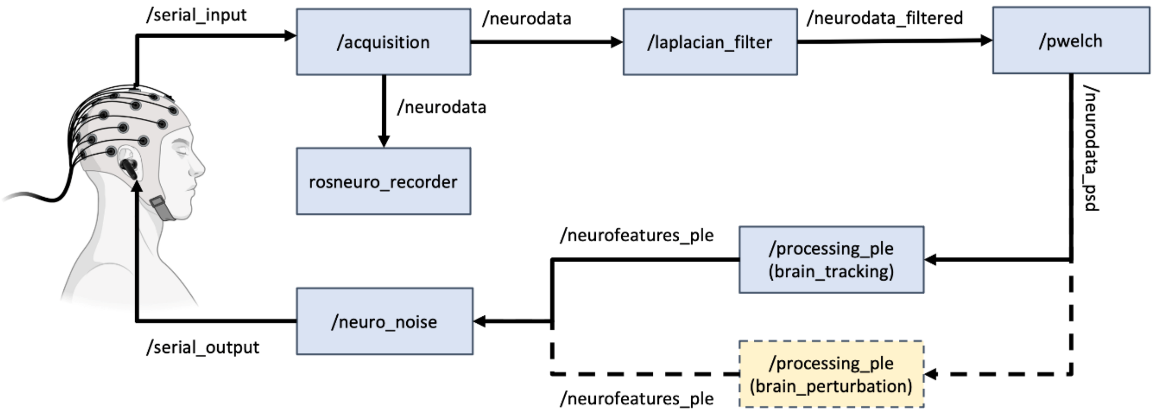

Fig. 2.1: Representation of the various nodes and topics that allow the realization of the passive auditory NFB. In addition, in the dashed line, you can see a node not yet developed but that will be subject to further development of the Neurofeedback presented here.

The system, depicted in Fig. 2.1 is developed through a closed loop that starts with the acquisition of EEG signals from different areas of the brain and aims to generate a sound proportional to the brain activity. The pipeline, after signal acquisition, provides filtering to increase spatial resolution, PSD calculation to observe signal strength in frequency domain, PLE calculation and generation of the noise. The different materials and methods used for this purpose are listed below, with a detailed analysis of all physical and computational aspects. The EEG cap used for signal acquisition and the software used for NFB implementation are described. The different complexity metrics used for research are illustrated and the different nodes that make up the signal processing to the realization of sound are analysed. The ultimate goal of the project is to perturb the brain activity in order to achieve wave modulation so as to normalise the activity of people with cognitive disabilities. The first part of the project involves generating a sound proportional to activity through tracking brain waves using a complexity index. The hatched part will then be developed into a future work that will trace brain activity and vary the complexity metric used to perturb it.

2.2 EEG cap

The EEG cap used is the Original Waveguard produced by ANT Neuro and it offers the technology of the Ag/AgCl material, that is light, flexible and sintered, which makes it easily usable with different heads. This headset, and especially the use of sintered Ag/AgCl, allows to record the EEG signal with great quality. The EEG cap is very easy to apply. For the attachment of the headset there is a chin strap. Two measurements are made by means of a tape measure for the location of the CZ electrode. To find the right location for the placement of the CZ electrode, the distance between the Nasion and the Inion was taken and divided by two and the distance between the left and right ear was calculated and divided by two. The point of meeting between the halves of the two measurements will be the location of the CZ electrode. The contact between the electrodes and the subject's head is made by a conductive gel that is applied with a blunt needle syringe. The needle is inserted into the electrode and the gel is squeezed until a good signal acquisition is achieved. The EEG headset adheres to the 10-20 system for electrode placement. The EEG cap used contains 64 electrodes.

Fig. 2.2: Picture taken during the experiments in the laboratory showing a subject under auditory NFB. In the picture is shown the EEG cap with 64 electrodes, an image shown at screen and headphones for auditory feedback.

2.3 ROS and ROS-Neuro

The Robotic Operating System (ROS) was used to implement the NFB. ROS is an open-source middleware designed for robotic applications that allows communication between different programs (nodes) through a communications infrastructure based on topics. ROS provides a standard and efficient communication between nodes This modular architecture allows drivers, sensors and processing algorithms to be developed independently and then easily integrated. ROS in addition to the concept of modularity introduces the notion of distributed computing making it possible to execute different processes on different machines sharing data in real time and thus allowing the development of more complex systems.

ROS uses a publisher-subscriber model in which different programs, called nodes, communicate with each other by publishing and subscribing data. Some nodes produce data that is published in a topic, while others acquire such data by subscribing to the topic. This allows for flexible and efficient communication. Nodes are usually programs that perform calculations, and each node handles a single specific task allowing for modular development. Packages are directories containing source code and configuration files. The ROS Master is a key part of integration and manages communication between nodes by keeping track of which nodes are publishers and which subscribers and to which topics making or extracting data. The ROS Master, therefore, allows the correct sorting of messages. ROS is used in various fields such as autonomous driving vehicles, industrial automation, drones and in recent years also in BCIs thanks to the introduction of ROS-Neuro [39, 40, 41]. ROS-Neuro is designed to bridge the gap between BCI and robotic systems. The main objective is to simplify the development of BCI applications that interact with robots or other devices in real time. ROS-Neuro also has a modular architecture. The acquisition node allows to interface hardware devices, such as EEG amplifiers, to acquire brain signals by providing standards for raw signal acquisition. The processing node applies filters to remove noise such as muscle artifacts, motion artifacts or electronic interference. Typically, spatial filters or frequency domain filters are implemented in this module. Finally, for closed-loop BCIs, feedback is essential to provide the subject with information about what is happening. Tactile, auditory or visual feedback mechanisms are implemented in ROS-Neuro allowing the user to regulate and modulate his brain activity. In the field of neurofeedback, ROS-Neuro allows the user to have real-time feedback for cognitive training, mental health treatment and rehabilitation.

2.4 Processing

The processing of the EEG signals is a crucial process during the development of an NFB as it allows for cleaner and more explanatory signals of brain activity. Raw data often contains artifacts and noise that complicate the interpretation of neural activity. Therefore, filtering techniques are usually implemented to improve the quality of EEG data and extract significant characteristics. Among these techniques, Laplacian filtering and the Power Spectral Density (PSD) calculation play an important role in the analysis of an EEG signal as they allow a pre-processing of the signal and the features extraction. Laplacian filtering is a spatial filtering technique that allows to improve the spatial resolution by reducing the effects of volume conduction. The PSD is a representation of the power distribution of a signal between its frequency components. For EEG signals, which consist of oscillatory activity over several frequency bands, the PSD analysis provides information on the functional states of the brain.

Laplacian filtering and PSD analysis address several aspects during the analysis of an EEG signal. Laplacian filtering improves spatial resolution and reduces artifacts while PSD focuses on the spectral content of signals. The two techniques increase data quality and interpretability of its features.

2.4.1 Laplacian filtering

Spatial filtering allows for an increase in the spatial resolution of EEG data. The EEG signal recorded by an electrode also contains activity from nearby brain regions due to the volume conduction effect. By applying this filtering, the signal spread is reduced by highlighting the differences between the different channels. In addition to avoiding the overlap of electrical activity from adjacent channels, Laplacian filtering minimizes low-frequency noise, reduces muscle artifacts and other sources of interference. Being computationally fast it is often used in real-time application. To perform Laplacian filtering, it is necessary to construct a matrix of weights, which will then be multiplied by the vector containing the values, at an instant in time, of the EEG signals from the different channels. The Laplacian matrix is constructed from the positions of the electrodes on the EEG cap. The channel considered is assigned a value of 1, while adjacent channels are assigned a value that corresponds to the unit divided by the number of adjacent channels. If the channel under consideration has four adjacent channels, then these channels will be assigned the value -1/4. This subtracts 1/4 of the value of that channel from the value of the channel taken into consideration and so also for the other three neighbouring channels. For example, if we consider the image below in which the C3 channel is considered and on which the cleaning by spatial filtering is carried out, we will have that to the value C3 weight 1 is associated while to the electrodes FC3, C1, CP3 and C5 it is assigned a weight -1/4. The mathematical formulation is:

$$C3_{filtered} = 1 * C3 - \frac{1}{4} * (\mathrm{FC3} + \mathrm{C1} + \mathrm{CP3} + \mathrm{C5})$$

FC5	FC3	FC1
C5	C3	C1
CP5	CP3	CP1

Fig. 2.8: Matrix portion of the electrode distribution around C3 of the EEG cap.

2.4.2 PSD, Welch method and 1/f trend

Usually, the Welch method is used to calculate the PSD, which breaks down the signal in the time domain into its frequency components and shows their power distribution. The steps for calculating the PSD using this method were designed to make the results less prone to noise and to reduce variance making the results much more reliable. Consider a portion of the total signal $x[n]$ of length N. The first step is to divide this portion of the signal into overlapping segments in the time domain. Consider that the signal is divided in K segments. Typically, the overlap is 50%, so if a window contains L samples the overlap will be $L/2$ samples. This step is very important to reduce the variance of the estimate. After dividing the portion of the signal into windows, a window function $w[n]$ is used for each segment to minimize the edge effects that can introduce spectral leakage in the FFT. The spectral leakage occurs when a spectrum of a signal is spread across multiple frequency bins instead of being concentrated at a specific frequency. This happens when the signal is sampled over a finite period. The most used window functions are the Hamming, Hann or Blackman windows.

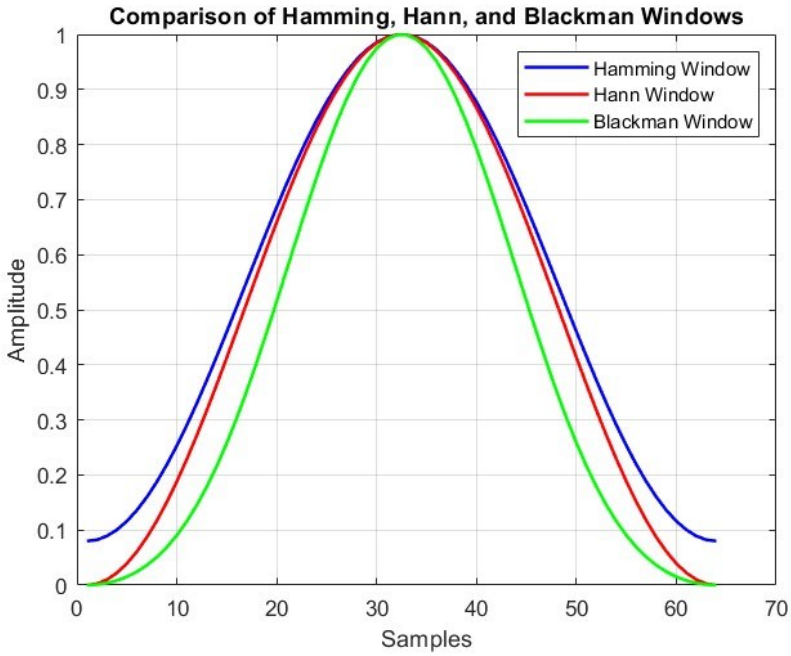

Fig. 2.4: This image represents the comparison between the three windows usually used for segment windowing. The difference between the 3 is in the aggressiveness at the edges and the width of the central lobes. The Hamming window is the window that makes the windowed data as close as possible to the initial ones. The Blackman window is the most aggressive and completely resets the values at the edges, also modifying the most central values.

The windowed segment becomes:

$$x_k[n] = x\left[n + k * \frac{L}{2}\right] * w[n]$$

$$for\ n = 0, 1, \dots, L - 1$$

The third step is to calculate the periodogram of the signal. The periodogram is the estimate of the spectral density of the signal. The result can be obtained by using the FFT of the windowed segment considered.

$$P_k(f) = \frac{1}{L * U} |FFT(x_k[n])|^2$$

$$U = \frac{1}{L} \sum_{n=0}^{L-1} w[n]^2$$

Where $P_k(f)$ is the periodogram estimate, U is the normalization factor that accounts for the power loss due to windowing. The FFT transforms the segment from time-domain to the frequency domain. $|FFT(x[n])|^2$ represents the power at each frequency. The last step involves averaging the periodograms of the windowed segments for the portion of the signal considered to obtain the final estimate of the PSD.

$$\hat{P}(f) = \frac{1}{K} \sum_{K=0}^{K-1} P_k(f)$$

Where $\hat{P}(f)$ is the mean of the periodograms that is the PSD, K is the total number of segments and $P_k(f)$ is the periodogram of the k-th segment. The frequency resolution depends on the length L of the segment taken and on the sampling frequency of the signal. If I take a segment of greater length I will have a greater resolution. The parameters to consider when applying this method are the length of the segment L which allows to adjust the resolution of the PSD. The overlap percentage also affects the computational cost of the algorithm, if in fact the value is increased more samples are taken into consideration for each signal segment thus calculating more periodograms for each segment. The type of windowing affects the spectral leakage. When examining the EEG signal in the frequency domain and then analysing the PSD of the signal, a 1/f trend is observed which refers to the way in which the signal power decreases as the frequencies increase. The PSD of the EEG signal represents the distribution of power at different frequencies. The 1/f trend can be interpreted as a reflection of the complex dynamics of neural oscillations. In fact, this trend suggests that the activity of neurons does not have a dominant rhythm but rather involves many interactions on different time scales that extend from milliseconds to seconds corresponding to high and low frequencies respectively. Brain rhythms and the 1/f trend can also be explained both by the balance between excitation and inhibition and by the synchronization of neural populations that align their activity producing low-frequency oscillations. As desynchronization increases, however, a decrease in power at high frequencies corresponds. There are many causes that can lead to a departure of neural activity from the 1/f trend. In some pathological conditions such as epilepsy the trend flattens indicating high activity at high frequencies. Other pathological conditions instead make the trend steeper indicating less neural involvement and a general slowing of the oscillations. The 1/f trend suggests that brain activity is organized in a fractal way and the trend reflects the brain's ability to manage information on multiple time scales. A 1/f trend is common in subjects in which there are normal psychophysiological conditions [46].

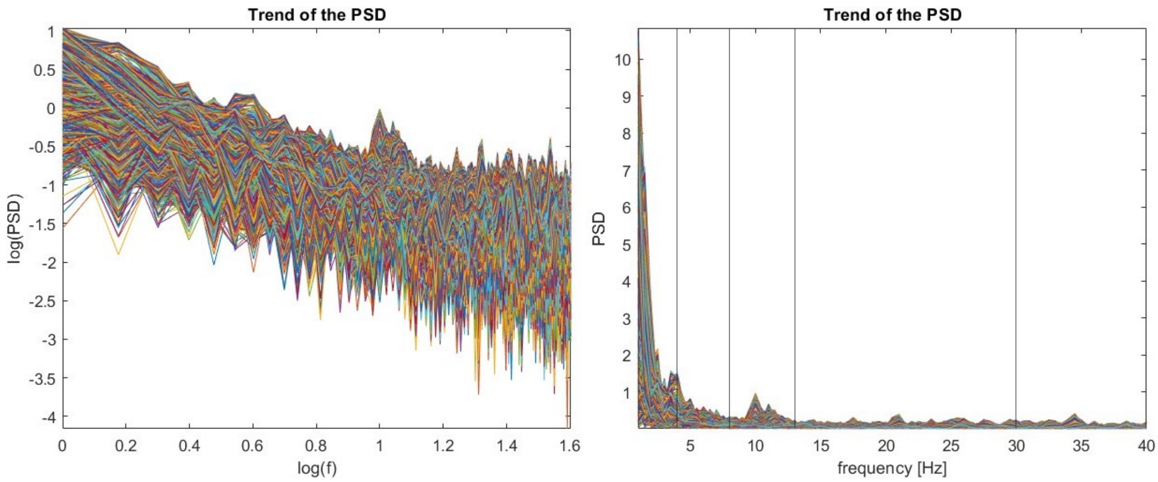

Fig. 2.5: On the left the 1/f trend of the PSD in the loglog graph. On the right the trend of the PSD with the peaks in the Alpha and Beta bands.

2.5 Complexity measures

Complexity measures in EEG analysis quantify different aspects of signal variability, organisation and spectral distribution. These measures make it possible to identify whether a subject's brain activity is within physiological norms or is in a pathological state. These metrics are very useful because they provide various information on the trend of the power spectrum of the EEG signal over time. In several studies it has been noted how the integration of different complexity metrics allows to obtain more information regarding the complexity of the EEG signal in the frequency domain. These metrics are able, differently from each other, to describe a complex aspect of the signal spectrum. In this work therefore they are compared to have a greater insight into the subject's brain activity and the relationship between them. This thesis explores the analysis of several complexity metrics including the Spectral Entropy, the Spectral Asymmetry Index, the Band Power Ratios and the Relative Power.

2.5.1 Spectral Entropy

Spectral entropy (SE) is a complexity measure often used in EEG analysis to assess the power distribution across different frequency bands. The SE provides information about the randomness of the signal, and this allows to determine the levels of consciousness and subject's brain states. The measure is derived from Shannon Entropy and is calculated based on the normalised Power Spectral Density (PSD). The computation of the SE involves calculating the PSD. The signal from the time domain passes to the frequency domain. Once the PSD of the signal is computed, it is normalised to have the probability distribution of the frequencies:

$$p(f) = \frac{P(f)}{\sum_f P(f)}$$

Finally, the Shannon Entropy is calculated using the normalised PSD:

$$SE = -\sum_f p(f) * log_2(p(f))$$

SE highlights the uncertainty or randomness of the EEG power distribution in frequency domain. High entropy values indicate a more complex and therefore more random distribution. In the field of BCI, higher values in certain cranial areas enable the subject to move robotic prostheses, for example. In the field of diagnosis, it is often used to monitor the deep sleep state during the administration of anaesthesia in surgical practices. If low entropy values persist during EEG recording, this means that deep sedation is taking place, and this allows the anaesthetist to adjust dosages in real time. For the detection of epileptic cases, the human brain assumes more deterministic patterns, resulting in a decrease in SE values. SE is also used in other diagnostic cases such as for monitoring neurological disorders, for detecting fatigue or cognitive load; all of which involve a change in non-physiological brain activity. SE is a metric that presents excellent prerequisites for its implementation in a BCI application due to its computational efficiency. The calculation of PSD is fast, and the calculation of entropy based on PSD involves the use of simple mathematical formulas. Indeed, in a BCI context, where an increase in concentration is required, a decrease in SE in certain frequency bands could be detected by providing feedback with minimal delay. The main problem that arises with the use of SE, however, is the variability of the results. The interpretation of these is too wide. Consider high entropy: this could be associated either with a state of relaxation, in which there is a desynchronised EEG, or with cognitive disorganisation as during an epileptic seizure. The ambiguity of the expected results makes it difficult to use SE alone in feedback scenarios in which the stimuli may be different. Although SE therefore measures overall signal complexity, it does not provide detailed information on neural mechanisms. Its usefulness, therefore, remains limited in a real-time NFB application due to the lack of specificity for different mental states, but it could certainly be coupled with other metrics for more adequate feedback. [6]

2.5.2 Spectral Asymmetry Index

The Spectral Asymmetry Index (SASI) is a complexity measure used in EEG analysis to assess the relationship between the high and low frequencies of the signal. This coefficient is used to determine whether there are abnormal asymmetries that may indicate suboptimal neurological conditions. The calculation of SASI involves four main steps. The first is the calculation of the PSD of the signal; the second is the selection of the frequencies used as boundaries; the third is the calculation of the PSD for the two selected bands and finally the SASI is calculated. The formula to compute the SASI is:

$$SASI = \frac{P_{high} - P_{low}}{P_{high} + P_{low}}$$

$$P_{high} = \sum_{f=13}^{100} P(f)$$

$$P_{low} = \sum_{f=0.5}^{13} P(f)$$

Where $P(f)$ is the total PSD of the signal, P_{high} is the power of the high frequency components (usually between 13 Hz and 100 Hz) and P_{low} is the power of the low frequency components (usually between 0,5 Hz and 13Hz). To ensure a fair balance, the bandwidth of the high frequencies is greater than that of the low frequencies because the EEG spectrum has a higher PSD at low frequencies than at high frequencies. The index has a range from -1 to 1 where positive values indicate a predominance of high frequencies while negative values indicate a dominance of low frequencies. A well-balanced symmetric spectrum has SASI values around 0. SASI is widely used in clinical settings to assess the balance of brainwave activity in EEG recordings. In the detection of epilepsy, an increase in SASI is often seen as there is an imbalance in the frequency bands and especially an increase in high-frequency activity. Another field of application is the detection and diagnosis of cognitive disorders where there is a shift towards slower activity with the index becoming negative. In the field of BCI, the SASI can provide continuous feedback on the balance between high and low frequencies allowing the subject to modulate their activity. The speed of the index calculation could be very useful in NFB practices where real-time feedback is needed. The main problems with the SASI are its complex interpretation as it only provides information that an imbalance has occurred but does not give us information on how this imbalance occurred. There is also a problem in the choice of the limiting frequencies that are used to calculate the sum of the PSD in the limited frequency bands. A standardised protocol would be needed for the use and comparison of the results of this index [42, 43].

2.5.3 Relative Power

Relative Power (RP) is a complexity metric often used in EEG analysis as it quantifies the proportionality of the power of a specific frequency band to the total PSD. To calculate the RP for each frequency band (RP_i), the total PSD of the signal (P_{tot}) and the PSD for each specific frequency band (P_i) must first be calculated.

$$RP_i = \frac{P_i}{P_{tot}} * 100$$

In real-time applications of NFB the use of RP can become advantageous for identifying and training specific cognitive states by allowing the subject to observe how brain activity varies over time. As in other cases, variability in brainwave patterns may influence the effectiveness of using RP in NFB applications where a calibration and training protocol would be required to ensure the reliability of the metric. Since this metric has too many features (five when considering the Delta, Theta, Alpha, Beta and Gamma bands) at the output, it was not considered for the purpose of this auditory NFB generation protocol. Furthermore, as there was no single index, it was not possible to create proportional noise that mimicked the PSD trend of the signal directly [7, 44, 45].

2.5.4 Band Power Ratios

Band Power Ratios (BPRs) are metrics that calculate the ratio of power of one frequency band to another by providing a ratio that reflects the relative contributions of different frequency components. They are usually used in the analysis of EEG to study different brain states and processes as they are described by power variations in frequency bands. These ratios are particularly effective for understanding functional connectivity and brainwave transition states. The formula for calculating a ratio in frequency bands is:

$$BPR_{B1-B2} = \frac{P_{B1}}{P_{B2}}$$

Where BPR_{B1-B2} is the power band ratio between the B1 and B2 bands, $P_{B1}$is the power in B1 frequency band and $P_{B1}$is the power in the B2 frequency band. B1 and B2 can be the bands Delta, Theta, Alpha, Beta and Gamma. In real-time applications for NFB, BPRs can be used by providing the ratio between two frequency bands. Each ratio indicates different mental, emotional and physiological states. A high ratio of the Theta band to the Beta band is most often associated with ADHD and attention disorders [13, 15, 29]. Reduced ratio values occur during cognitive recruitment and high attention states. A high ratio between the Theta and Alpha bands can be associated with drowsiness, a lack of focus or cognitive recruitment and is usually observed in subjects with attention deficit or cognitive load. A lower ratio, on the other hand, is associated with states of relaxation and focused attention. Lower values following NFB treatment may indicate improved cognitive performance and concentration [13, 21]. A high ratio of the Delta band to the Alpha band indicates a state of cognitive impairment and dementia. There are also ratios that allow us to understand what emotional state the patient is in during the signal acquisition, and these are indices that will be considered during the experiments especially in the analysis of the results obtained. A high ratio between the Alpha band and the Beta band allows us to understand if the subject is in a state of relaxation while a low ratio indicates a level of stress [26] or anxiety [13, 37].

2.5.5 Power Law Exponent

The Power Law Exponent (PLE) captures the overall PSD trend of the EEG signal. To compute the PLE, it is necessary to apply the logarithmic transform to both the frequencies and the PSD. Usually, the PSD trend in frequency follows a 1/f trend. By applying the bi-logarithm transformation, the PSD trend becomes linear. The PLE is then computed by linear regression on the frequency and PSD data transformed. The linear fit returns two values: the intercept with the vertical axis and the angular coefficient of the regression line. The angular coefficient is the PLE. The linear regression is done via the method of least squares. The objective is to find the best-fitting line across a large amount of data. The line can be described by the following equation:

$$y = m * x + b$$

Where y is the predicted value or dependent variable, x is the independent variable, m the slope of the line and b the intercept. To derive the slope m and the intercept b given a set of points $(x_1, y_1), (x_2, y_2), \dots, (x_n, y_n)$, where n is the amount of data, the method of least squares minimises the sum of the squared differences between the observed data and the values predicted by the regression line. The error for each point is:

$$Error_i = y_i - \hat{y}_i$$

The objective is to minimise the sum of the squared errors:

$$S(m, b) = \sum (Error_i)^2$$

To minimise this function, the partial derivatives of $S(m, b)$ with respect to m e b are calculated. The partial derivatives are set to zero and by solving the two equations we obtain the equations to find m and b.

$$m = \frac{n \sum(x_i y_i) - \sum x_i \sum y_i}{n \sum x_i^2 - (\sum x_i)^2}$$

Once m has been found, the intercept b is calculated according to the following formula.

$$b = \frac{\sum y_i - m \sum x_i}{n}$$

Once m e b have been calculated, the linear regression equation becomes:

$$\hat{y} = m \cdot x + b$$

Of the two coefficients found, we are interested in m which corresponds to the value of the negative of the PLE if the regression is performed on the PSD data. For sound generation, we will take a negative value of the angular coefficient. considering that the general trend of the PSD is 1/f the angular coefficients that will come out of the linear regression on the PSD will always be negative. So, we will assume that the PLE is the negative of the angular coefficient of the linear regression line.

$$PLE = -m$$

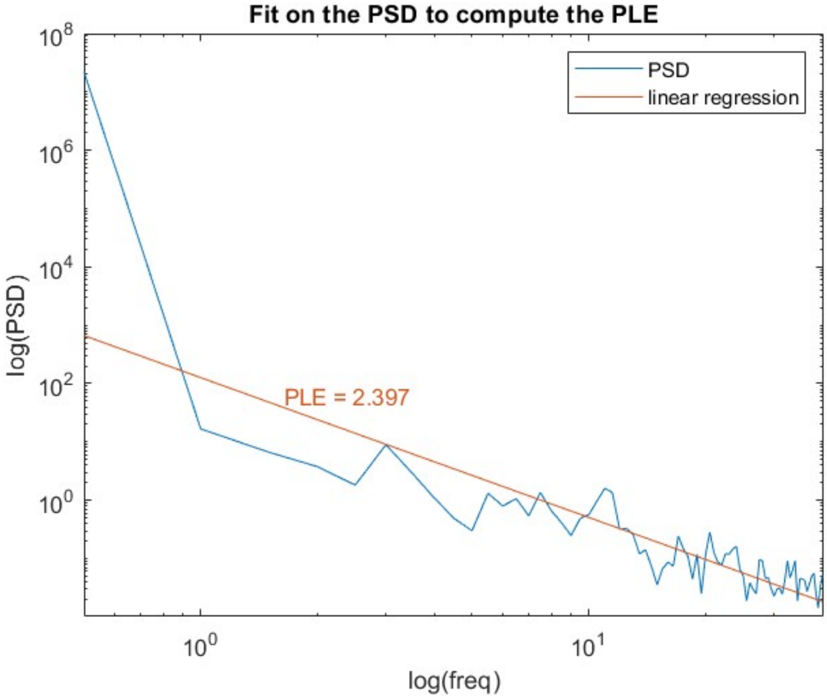

Fig. 2.3: In this figure, the linear regression fit on the PSD is observed, brought to a logarithmic scale. The PLE is positive because it is the negative of the angular coefficient of the line. This image was obtained by recording an EEG signal and calculating the PSD on a 4-second portion of the signal using the Welch method. Subsequently, a transformation to a logarithmic scale was made, using the logarithm to the base of 10, both frequency axis and of the PSD values, and a linear fit was made on the new PSD values.

Offline simulations have shown that this coefficient is able to capture the trend of brain activity well, despite being very susceptible to minimal variations. The PLE allows capturing not only the trend of a specific frequency band, but rather the entire complex structure of EEG frequency activity [18, 20, 35, 36].

2.6 Coloured noise

Coloured noise refers to all types of colours that are not white noise or with PSD varying with frequencies. The PSD usually follows a trend inversely proportional to the frequency high at a factor:

$$S(f) \propto \frac{1}{f^{\alpha}}$$

Where α is a positive or negative number. For values of α equal to 1 and 2 we have pink noise and brown noise respectively. The value of α then determines how much content is maintained at high frequencies. If α assumes positive values, there will be a reduction in the high frequencies, whereas for negative values of α the energy at the high frequencies increases. For values of α equal to -1 and -2 we have blue and purple coloured noise, respectively. Frequency trend is an important concept because many systems in nature behave in this way.

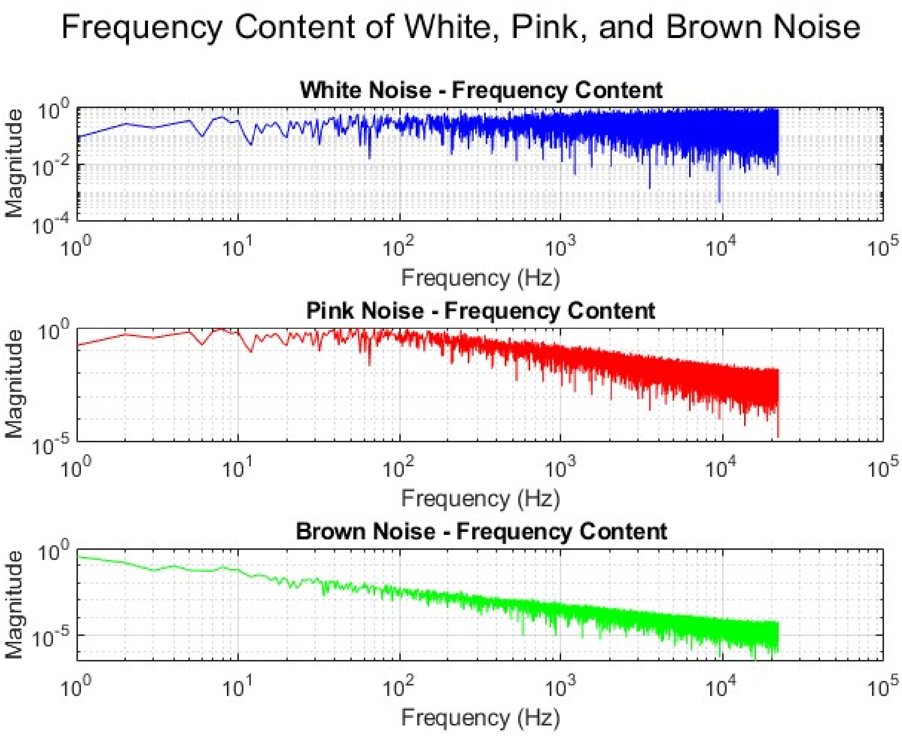

Fig. 2.6: White, pink and brown noise patterns. You can see that with increasing frequency there is a lower power decay for the pink noise and a greater decay for the brown colour.

2.6.1 White noise

White noise is a signal with the same intensity at all frequencies. Investigating its spectral density, we notice how it is flat over the whole frequency range. If we define its PSD as S(f) then:

$$S(f) = C$$

with C constant independent of frequency f. In the time domain it appears instead as a sequence of random and unrelated values. The autocorrelation function is a delta Dirac function, which means that it has no correlation at different time points.

$$R(\tau) = \delta(\tau)$$

Where R(τ) is the autocorrelation function and δ(τ) is the Dirac delta. The sound perception of white noise is similar to that of a continuous rustle, and this is due to the fact that all audible frequencies are present at the same power without favouring a certain frequency band. The high frequency content makes white noise less pleasant than other noises, like pink or brown, which have a low content at high frequencies. The discrete white noise e[n] can be modelled by a finite sequence of random values:

$$e[n] = A * q[n]$$

Where A is the amplitude of the noise, q[n]is a random number extracted from a distribution which can be for example gaussian or uniform and the discrete time index. The assumptions made on the white noise model are stationarity and ergodicity. Stationary signal means a signal that has statistical properties which are invariable over time. Signal parameters such as mean, variance and autocorrelation thus remain constant over time. Ergodicity implies that statistical properties can be determined by observing a single temporal realization of the signal over a long period of time. White noise can be used for signal processing applications, testing and simulations, communication channel models and noise masking [35, 36].

2.6.2 Pink noise

The pink noise is characterized by a PSD that decreases with increasing frequencies following a 1/f trend. This pattern makes lower frequencies more noticeable than higher ones, creating a more pleasant noise than white noise. The perceived noise is like that of the rustling of wind through trees, the noise of sea waves or constant rain. In the frequency domain we can say that the PSD is proportional to the inverse of the frequency:

$$S(f) \propto \frac{1}{f}$$

Where S(f) is the PSD and f is the frequency. For each octave, then the power decreases by 3 dB. Octave means a doubling of the frequency. The frequency trend reflects a balanced distribution between low and high frequencies. Unlike white noise which theoretically contains infinite energy given its flat spectrum, pink noise has finite energy due to the decrease in power as frequencies progress. In the discrete time domain, pink noise is created by applying a low pass filter to white noise trying to mimic the natural pattern of pink noise. Applications of pink noise include audio testing, background masking, relaxation techniques, sleep aids, music and sound design [35, 36].

2.6.3 Brown noise

Brown noise is characterized by a PSD that decreases with increasing frequencies. Its decrease follows a slightly different trend from the pink colour. In fact, the PSD is inversely proportional to the square of the frequency:

$$S(f) \propto \frac{1}{f^2}$$

Where S(f) is the PSD and f is the frequency. This implies that for every frequency doubling the power decreases by 6dB and this leads to a higher concentration of energy at low frequencies and a rapid decrease in energy at high frequencies. Mathematically the brown noise is created by applying a low pass filter to white noise trying to mimic the frequency trend. The bass is dominant during the perception of brown noise with softer transitions than white noise. The fact that it has a very low energy at high frequencies makes the brown colour similar to a deep hum that has a calming and stabilizing effect. Brown noise is found in the same applications as pink noise [35, 36].

2.7 Nodes

The code implemented in ROS, whose structure is shown in Fig. 2.7, consists of nodes communicating with each other through topics.

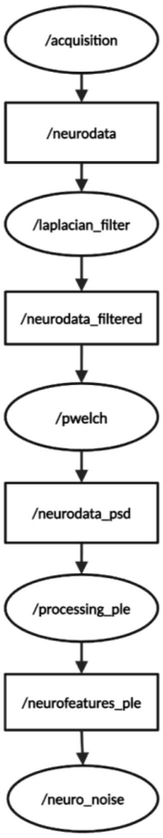

Fig. 2.7: Representation of the signal processing pipeline from acquisition to noise generation through nodes and topics generated in ROS. Ovals represent nodes and rectangles represent topics.

The first node is the EEG signal acquisition node */acquisition*, which publishes data to topic /*neurodata*. The data is then read by the subscriber /*laplacian_filter* who performs the spatial filtering of the signal. The filtered data published in topic /*neurodata_filtered* are sent to the /*pwelch* node that deals with the calculation of the PSD. Then, in the /*neurodata_psd* argument, the calculated PSD values are published and read by the/*processing_ple* node that compute the

PLE. Finally, the PLE values contained in */neurofeatures_ple* are read by */neuronoise* and, through the generation of sound pieces, an auditory feedback is produced.

2.7.1 Acquisition node

The acquisition package provided by ROSneuro provides an interface for data acquisition from different devices. In this case we used the *eegdev* plugin which is an interface to access various EEG systems designed to be flexible and efficient. The package acquires data from the sternal device and publishes it as a *NeuroFrame* message represented by a sample size data block for channels. In this work a sampling rate of 512 Hz was used, and the acquisition is set to have a framerate of 16Hz which implies that each *NeuroFrame* will contain 32 samples for the number of channels (in this case 64).

2.7.2 Laplacian node

The Laplacian node is used to perform a spatial filtering to reduce the effect due to nearby channels. To perform the spatial filtering, the vector of the samples from the 64 channels must be multiplied by the matrix containing the Laplacian mask. To carry out the filtering, a 64 x 64 Laplacian matrix was built that contained the linear combinations of all 64 channels resulting from the EEG acquisition. The channels are then multiplied with this matrix and the filtered signals are obtained, ready to be processed by the PSD calculation node.

2.7.3 PSD node

In this node the PSD calculation has been implemented. For the calculation of the PSD, we used the method of Welch. The parameters needed for calculating the PSD in a time window are different. First, the number of samples for a four-second signal time window must be provided. Usually, a 1 second window is used so that you do not have too much signal information passed. It was necessary to use a window of four seconds, however, because to go and analyse the signal at low frequencies it was necessary to take a longer time of observation. In fact, if the observation period (T) is four seconds and the sliding window to compute the FFT is two seconds the lowest observable frequency is 0.5 Hz from the formula:

$$f_{min} = \frac{1}{T_{sliding\_window}}$$

where $f_{min}$is the lowest observable frequency and $T_{sliding\_window}$ the observation period of two seconds that in our case is half of the period taken for the analysis. The second basic parameter is the sampling rate which is 512 Hz (f_s). Having these two parameters (T and f_s) it is possible to find the number of samples in the four second window and the maximum frequency visible by the frequency analysis. In fact, the number of samples in a four-second window is:

$$N = T * f_s = 4 * 512 = 2048\ samples$$

While the maximum observable frequency is:

$$f_{max} = \frac{f_s}{2} = \frac{512}{2} = 256\ Hz$$

In this case study these values are optimal for frequency analysis because the PLE calculation has been observed to be in the range 0.5 Hz - 40 Hz. The values of T and f_s are therefore optimal for a wider frequency range, higher resolution and more signal information. For the calculation of PSD, is needed to know the number of samples used for the calculation of PSD of the internal window that were 1024 corresponding to 2 seconds (*wlength*). Then is needed the number of samples used for the overlap that were 512 corresponding to 1 second (*noverlap*). Finally, is needed to specify the type of window used during the calculation of the FFT which in this case is the Hamming window.

T	*2048 samples*
f_s	*512 Hz*
wlength	*1024 samples*
noverlap	*512 samples*

Table 2.1: Values assigned to the variables necessary for the calculation of the PSD by the method of Welch.

2.7.4 PLE computation node

The PLE calculation code was implemented in this node. Frequencies from 0.5 Hz to 40 Hz were taken for the PLE calculation. This is to ensure that you take the most informative bands and to take the general trend of the PSD. Every 0.0625 seconds, the computed PLE value is published on the topic */neurofeatures_ple*. The value of the outgoing PLE is computed on the previous 4 seconds of EEG signal recording. In Fig. 2.9 it can be observed the PLE trend in time.

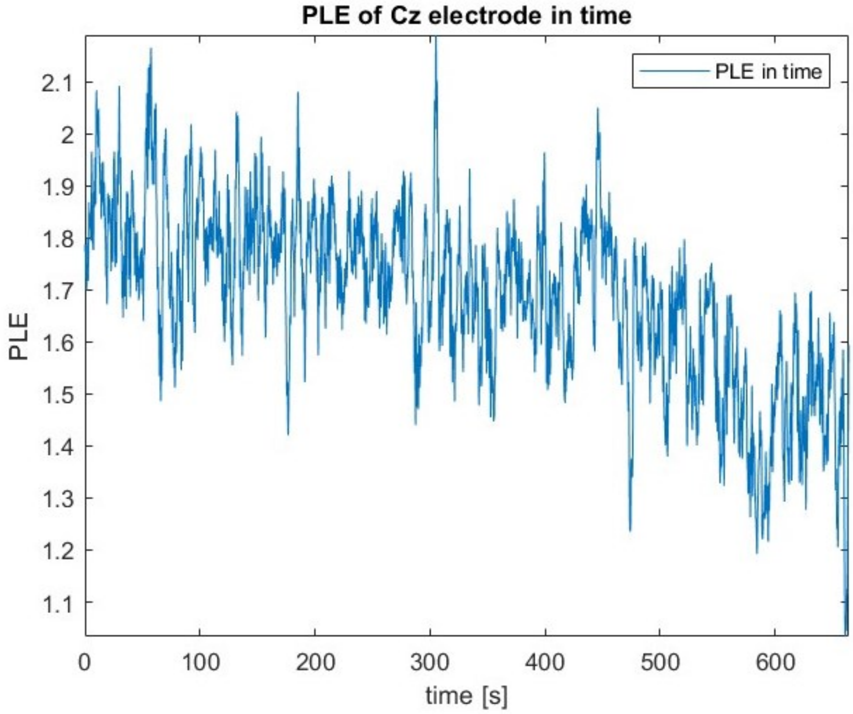

Fig. 2.9: Example of the PLE's trend in a ten-minute registration.

2.7.5 PLE to noise node

When a PLE value is published from the previous node, the node that generates the sound (*/neuro_noise*) subscribes to the topic (*/neurofeatures_ple*) and takes in input the new PLE values. In this node, the generation of noise proportional to the value of the PLE is implemented. Preliminary records showed that the variation of PLE is very high. This leads to an output with very marked variations. It was noted, however, that when observing the trend over longer time windows, PLE followed softer trajectories. To overcome this problem, exponential smoothing has been implemented. The only parameter used in this technique is the smoothing factor, which is defined as α. By using exponential smoothing you can modify this parameter to have a more or less smooth trend of the PLE signal. The exponential smoothing uses two values: the new value of PLE and the past value which is a combination of all the values preceding it. The formula for calculating the new value is:

$$PLE_{smoothed} = \alpha * PLE_{new} + (1 - \alpha) * PLE_{old}$$

where $PLE_{smoothed}$ is the new value of PLE that will be used for sound generation, PLE_{new} is the new value published by the PLE node and PLE_{old} is the old value used for the previous sound generation.

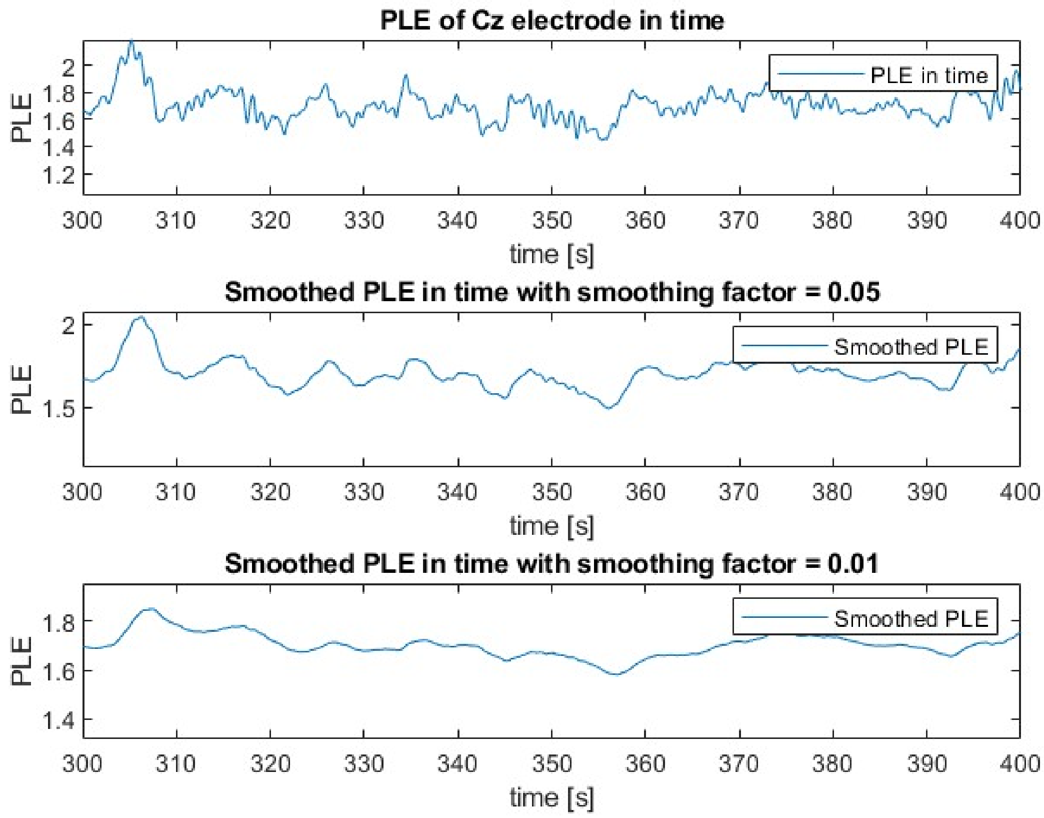

Fig. 2.10: Representation of the PLE over time with change in the value of the smoothing factor from 0,05 to 0,01. When the value of the smoothing factor decreases, there will be a smoother signal trend as the new value will have less influence on the trend.

Once the new PLE value is obtained, noise generation is carried out. First of all, the frequency axis was created using the sampling frequency of the generated noise ($f_{s_{audio}}$ equal to 44100 Hz) and the number of frames, i.e. the number of samples used for the sound generation. The number of frames is chosen according to the desired audio quality. In this case, the number of frames is 384 samples and is automatically chosen by the program. The number of frames could also be chosen higher, such as 512 or 1024, but it would make the generation of the noise difficult to manage by the program causing audio distortion. The sampling rate of 44100 Hz is chosen because it is the standard for CDs and other digital audio formats. This choice offers the possibility of covering the entire human auditory spectrum ranging from 20 Hz to 20,000 Hz. According to the Nyquist-Shannon sampling theorem, the sampling rate must be at least twice the maximum frequency present in the signal to avoid aliasing. So, to capture frequencies up to 20 kHz the frequency must be at least 40 kHz. The 44,100 Hz, therefore, provides a higher margin ensuring better audio fidelity. Using this frequency also simplifies integration with many external audio systems and devices such as speakers, headphones and sound cards. Following the frequency axis, white noise is generated which will be the basis of the process. To do this, a series of random values with a Gaussian distribution at mean zero and unitary variance is created. The signal strength will be equal at all frequencies. Then, the white noise

FFT is calculated. This step is used to bring white noise from the time domain to the frequency domain. The frequency components were then scaled by a scaling factor (sf). This scaling factor is used to convert the white noise into a coloured noise based on the current PLE value. The scale factor is calculated for each frequency as:

$$sf = |freqs|^{-\frac{PLE}{2}}$$

where sf corresponds to the scaling factor and $freqs$ to the previously generated frequency axis. If the PLE is equal to 1 the power decreases with frequency as in the case of white noise, while if the PLE is equal to 2 the power decreases faster as in the case of brown noise. The exponent divider ensures that the scaling of the amplitudes corresponds to the desired noise pattern based on the PLE value. The Fourier coefficients of white noise used for the generation of coloured noise are not directly the power values but represent the amplitude of the signal at each frequency. The power is proportional to the square of the amplitude of the Fourier coefficients. This means that the value of the PLE at the exponent must be divided by 2 when applying the scaling factor to the Fourier amplitudes to correctly reflect the power law trend. The divisor, therefore, ensures that the resulting signal will have the correct power spectrum pattern corresponding to the desired noise. Multiplying the scale factor to the FFT of white noise gives the coloured noise:

$$FFT_{colored_{noise}} = sf * FFFT_{white_{noise}}$$

Then, the inverse FFT is applied to transform the coloured noise from the frequency domain to the time domain and take only the real part.

$$colored_{noise} = real\left(ifft\left(FFT_{colored_{noise}}\right)\right)$$

The generation of each 384-sample chunk is generated instantly, and the different chunks are not connected to each other. This means jumps between sounds and thus a distortion of the audio noise making the sound unpleasant. To overcome this problem, an overlap between the chunk of the previous sound and the new one has been introduced. A window made up of 25% of the chunk samples is used to create a smooth effect between the sound sequences. In particular, a Hann window was adopted for a smoother crossfade. The idea is to extract the last part of the previous chunk segment and the first part of the next one and apply the fade-out and fade-in smoothing windows respectively. The fade-in smoothing window was calculated by taking the first half of the Hann window while the fade-out window was calculated by taking the second half of the Hann window. Crossfade is applied by combining the end of the previous segment with the beginning of the new segment using the fade-out and fade-in windows. The result is that the volume of the previous segment gradually decreases while the volume of the new segment increases creating a smooth transition.

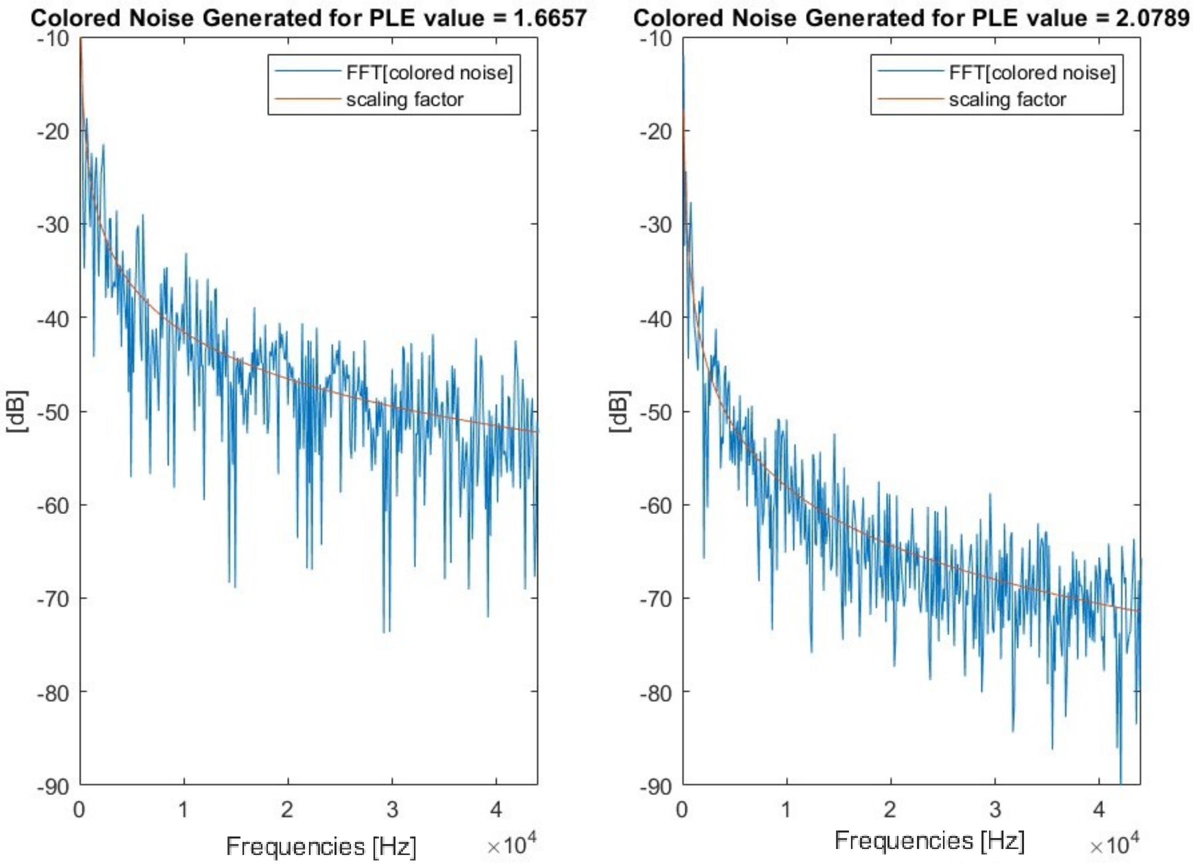

Fig. 2.11: Change in the slope of the trend of the coloured noise as the value of the PLE changes. The higher the PLE value, the more noise will be dropped at high frequencies producing a browner colour.

Chapter 3: Experiments and Offline analysis

3.1 Experimental protocol

To test the implemented NFB, several experiments were performed with acquisitions on healthy subjects. Five subjects were considered: four men and one woman. All subjects are young (all aged between 23 and 27) and have no certified cognitive impairment. The experiment proceeds along the pipeline described below. First, the EEG cap is connected to the power system and the system is connected to the PC. The subject is seated on a chair and has EEG cap placed over his head. The distances between the right and left ears are measured with a measuring tape, followed by the distance between Nasion and Inion. The measurements obtained are divided in half and the CZ electrode identifying the central scalp area is placed at the point where the measurements meet. Once the EEG cap is placed on the subject's head, the conductive gel for each of the 64 electrodes is inserted. For the display of the signal trend and signal cleaning, the visualizer offered by ROS-Neuro is used. The *neuroviz* visualizer is a GUI interface that allows visualization of electrical activity recorded by electrodes in real-time. Through this tool, we can check if the signal is clean enough or if there is a need to fix the quality of the signal. Once the gel is inserted into all 64 electrodes, the first experiment is carried out. For the experimental phase, a three-step protocol of recording brain activity was used.

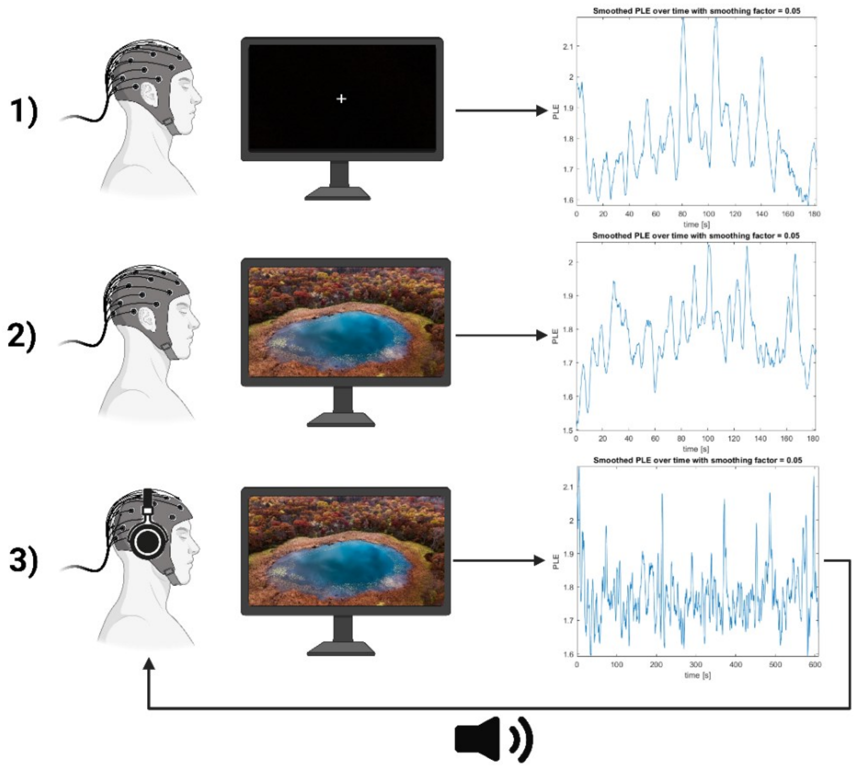

Fig. 3.1: Representation of the three phases of the protocol. The subject has the EEG cap on his head. The subject is watching a white cross in the first phase and images in the other two phases. The EEG signals are acquired, recorded and processed to obtain the PLE. The graphs in blue show the smoothed PLE values extracted in real-time from the subject EEG. For the first and second phases there is no auditory feedback. In the third phase, however, there is auditory feedback, proportional to the PLE value, delivered via headphones.

The first part of the three-minute protocol involves a white centre cross on a black screen (fixation cross). This image is submitted to the subject in an attempt to reduce noise from eye rolling artifacts. The subject is asked to fix the cross in the centre of the screen so that the eyes do not move and thus to reduce the artifacts from eye movement. This phase allows to record the brain activity of the subject in a resting state where no stimuli are provided and where the subject is asked to move as little as possible. This first calibration phase is used later as a baseline to investigate the change in brain activity of the two successive phases.

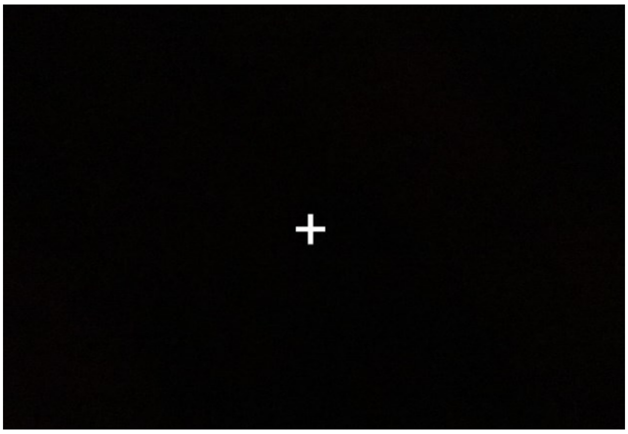

Fig. 3.1: Image displayed on screen during resting state.

The second phase of the protocol also lasts three minutes and, as in the third phase, involves the display of images which scroll on the screen. The images depict different natural landscapes. The only thing that is unique about these images is that they all have a central focus. In fact, the images displayed have been selected because they have a focal point located at the centre.

Fig. 3.2: Sample image of the images which are scrolled on the screen during acquisition in the second and third phases of the protocol.

This feature allows the subject to keep his eyes on the screen and to keep his gaze approximately fixed in the centre of the screen so as to avoid the effect of eye rolling. The image remains on the screen for six seconds and then the next image is introduced with a two-second fade. This part of fading and resting the image is essential to avoid the appearance of visual potentials due to the rapid passage of images. Again, no sound is emitted, and the brain activity of the subject is recorded to see if the images influence the subject's brain activity. The third phase of the protocol is longer and lasts ten minutes. The length of this part is due to the fact that we want to investigate the effect that the sound has over time. In this phase, in addition to the screen images, auditory feedback is also presented closing the loop of the NFB previously described.

3.2 Offline Analysis

The results obtained were obtained by offline signals analysis. The recorded signals are raw and therefore two analyses were made. The first analysis involves using the raw signal with the application of the spatial filter only. This analysis allows to mimic perfectly the PLE values over time that were used to produce the auditory feedback and thus to carry out an accurate analysis of the experiment. The second analysis involves the use of a more aggressive filtering by several techniques described below. The second analysis is used to investigate more deeply the course of brain activity of the subjects, also highlighting the pros and cons of a real-time application with such low content of signal filtering. Before starting with the analysis, a part of offline filtering was implemented to extract brain signals as clean as possible. First of all, the signals are filtered through a band pass filter with cut-off frequencies of 0.25 Hz and 45 Hz. This step is used to eliminate all the components of the signal that are not useful for the purpose of the experiment, and also allows noise to be removed at low frequencies and high frequencies. The Laplacian filter is then applied, as done in real-time, on the filtered signals. Then, the Independent Component Analysis (ICA) is calculated which allows to decompose the EEG signal into additive subcomponents under the assumption that these components are independent of each other and not gaussian [34, 37]. The ICA assumes also that the recorded EEG signals are a linear combination of statistically independent brain sources. To achieve source separation there are algorithms that allow maximising the non-Gaussian components and a common approach is to maximise the Negentropy. The assumption of non-Gaussian for sources is expected because if all sources were Gaussian then there would be no statistical independence. Non-Gaussian is often measured using indices such as Kurtosis or Negentropy. In our case, the index used was Negentropy. Negentropy measures how far a distribution of values is from a normal distribution and is defined as:

$$J(X) = H(X_{Gaussian}) - H(X)$$

where $H(X)$ is the entropy of X while $X_{Gaussian}$ is a Gaussian variable with the same mean and variance of X. The algorithm used in this work is FastICA. The ICA often produces results that vary from iteration to iteration. This is due to the nature of the algorithm that initializes weights differently and randomly thus varying initial conditions leading obviously to different results. In the case of FastICA, in fact, the initial weights of the unmixing matrix are initialized randomly. The algorithm then iterates from this initial point. To avoid that, a seed was set in the code that allows to start with the same initial conditions. The independent components are filtered by a low pass filter with a cut-off frequency of 40 Hz. This step allows you to filter all the high frequencies that are not useful. Not having signals from electromyographic sensors we have no information regarding facial and cranial muscle activity. Without this information we cannot eliminate the contributions from muscle activity. A good method of filtering these components is high frequency filtering to remove muscle artifacts. The final cleaning part involves removing the eye artifacts. In fact, recording the activity resulting from eye movement via EOG allows you to compare the EOG signal and the independent components. The comparison is done by linear regression and correlation of the EOG signal with all the independent components [34]. The components most affected by ocular artifacts are extracted by intersecting the results of regression and correlation. Finally, the independent components with higher beta, which is the weight associated with the amount of variance explained by the signal derived from linear regression, and higher correlation are eliminated. This filtering technique was used to obviate the selection by visual inspection of the components. In doing so, standardised signal processing was introduced to limit the error in the selection of components to be eliminated [37]. After the filtering of the signals, we proceed with the calculation of the PLE over time and then with the analysis of the signal. As a first analysis, the PLE was observed both raw and smoothed. Subsequently all the signals adjacent to CZ were displayed. To do this, a 5 x 5 mask with CZ in the centre was used and the PLE values for each of the channels present in this mask were extracted. Subsequently, to obtain a quantitative value of the similarity between the CZ channel and adjacent channels, the mean PLE of the channels was calculated and the mean signal was extracted. This allowed the correlation between the PLE signal from CZ and the mean PLE signal to be calculated by means of the Pearson correlation coefficient [15]. This step is to verify a real similarity between the general trend around CZ and CZ. The calculation of the Pearson coefficient is carried out by means of the following formula:

$$r = \frac{\sum(X_i - \bar{X})(Y_i - \bar{Y})}{\sqrt{\sum(X_i - \bar{X})^2} * \sqrt{\sum(Y_i - \bar{Y})^2}}$$

where X_i and Y_i are the sample values of the PLE signals, $\bar{X}$ and $\bar{Y}$ are the respective means of the two signals and r is the Pearson correlation coefficient. The coefficient has values ranging from -1 and 1 where 1 indicates a perfect linear relationship between the signals, -1 indicates a negative linear relationship and 0 indicates that there is no relationship between the two signals. After the correlation calculation, complexity metrics were investigated. To do this, since the metrics and PLE were on different amplitude scales, the data was normalized as the signals were comparable over time. For data normalization the mean of the signal was subtracted and each sample divided by the standard deviation, thus obtaining the normalization of the complexity signal. The transformation formula for each sample is:

$$z_i = \frac{x_i - \mu}{\sigma}$$

where z_i is the normalized sample, x_i is the sample value, μ is the mean of the complexity signals and σ is the standard deviation od the complexity signal. Once the complexity metrics are calculated, they are normalized and compared to the PLE performance to have a higher conception of the brain activity performance of the subject. The angular coefficient of the linear regression line calculated on the PLE signal over time in the CZ channel was then extracted. This practice has made it possible to understand whether there are consistent intra-subject or inter-subject trends. After having extracted the angular coefficient of the regression line and then after understanding if there was a general trend among the subjects, topographical maps were calculated. The topographic maps calculated are of two types. The first represents the average PLE signal path for each channel within the 5x5 mask around CZ. These maps were extracted to understand whether the PLE in the different channels changed intensity around CZ in the different protocol stages.

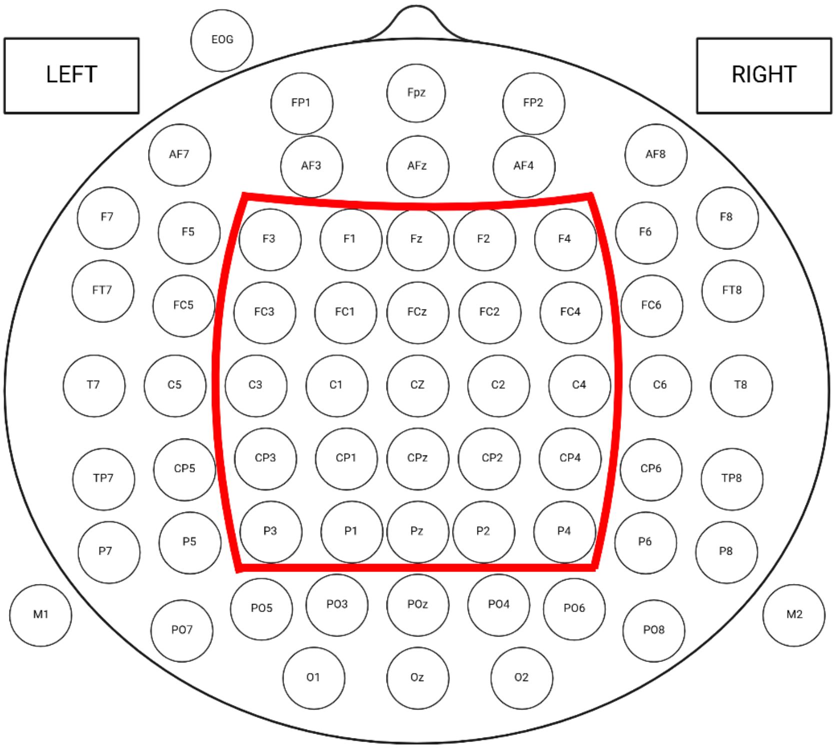

Fig. 3.3: Representation of the 5x5 mask used to compare the value of the PLE of the CZ channel and its adjacent channels for the representation of topographic maps.

The second one represents the PLE trend for regions of interest.

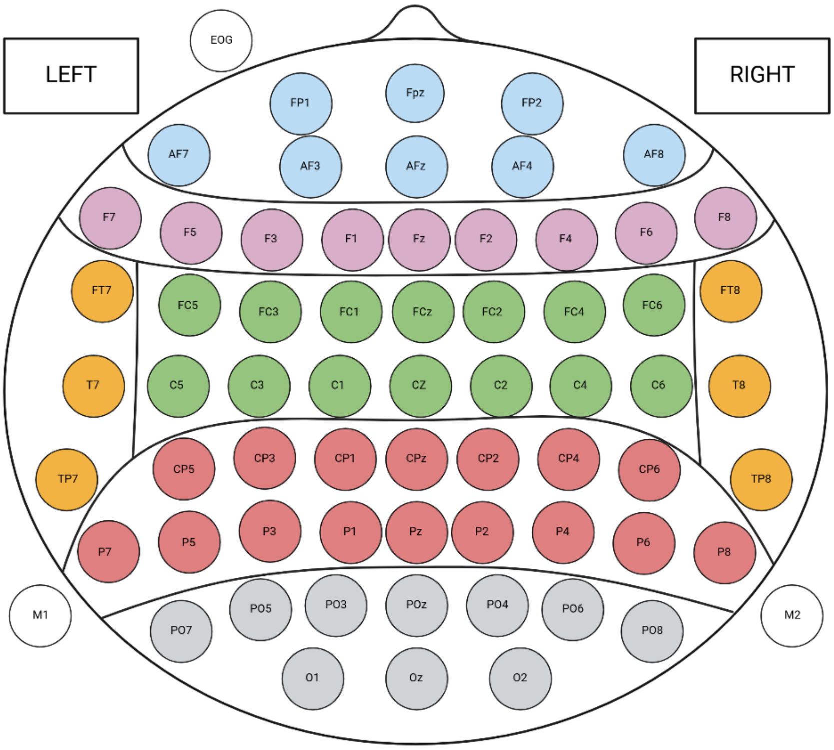

Fig. 3.4: Representation of the scalp subdivision into areas of interest (ROI) used for the calculation of topographic maps. In blue is represented the prefrontal area, in purple the frontal area. In green the central area, in yellow the temporal area, in red the parietal area and in grey the occipital area.

The scalp of the subject was divided into different zones: frontal zone, prefrontal zone, central zone, parietal zone, temporal zone and occipital zone. The average value of each channel over time was taken and then averaged between the channels in the area. Maps identify the average pattern of PLE in different brain areas. This measure is used to see if there is a recurring pattern between the different subjects. For the phase of the protocol in which sound is generated, the sound spectrogram has been displayed. In these images, it is possible to appreciate how, as the PLE increases, there is a greater decay of the sound frequencies' amplitude as the sound frequencies increase. Finally, the mean values and standard deviations of PLE signals in the CZ channel were calculated for each subject at each stage of the protocol during processing of unfiltered and filtered signals. This has served to further investigate the general trend of PLE in the CZ channel.

Chapter 4: Results and Discussion

The results obtained from the experiments allow us to further investigate the course of the brain activity of the subject. Different metrics were used for the time and frequency analysis of the signals obtained. The results obtained were derived from an intra-subject analysis to understand the dynamics of the PLE and the reliability of this measurement. In addition, an analysis was also carried out in which comparison indices were extrapolated between subjects to find recognizable inter-subject patterns. The following discussion of results aims to present a critical analysis comparing the results obtained before and after filtering in the three different phases of the protocol. The use of unfiltered signals allows for an understanding of the actual results obtained during the proposed protocol, examining the effectiveness of the applied filtering and the appropriate choice of parameters used in the development of codes for the implementation of the NFB. The analysis of filtered signals allows a deeper understanding of the intra-subject and inter-subject brain dynamics, highlighting possible common patterns between different brain areas. The discussion will use single-subject data as the intra-subject patterns and complexity metrics are the same in all subjects. The use of single subject results facilitates intra-subject analysis. For the inter-subject analysis, the results of the five subjects will be shown.

4.1 PLE raw and smoothed

The first analysis to be carried out is the trend of PLE over time. For the proposed NFB system, in fact, the actual value of the PLE obtained by linear regression of the PSD is not used; the value following exponential smoothing is used.

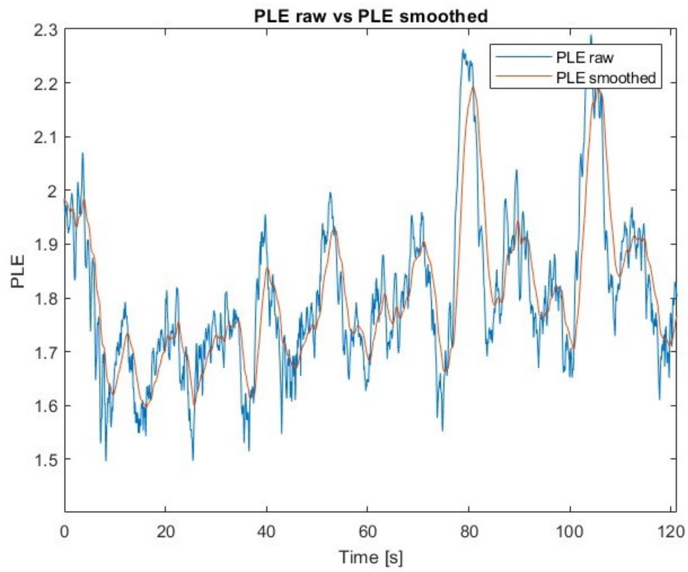

Fig.4.1: Comparison between PLE raw and PLE smoothed after exponential smoothing in the CZ channel. This graph is from the fifth subject and shows the PLE trend in the first phase of the experiment.

In Fig. 4.1, it is possible to observe the trend of the PLE before and after the exponential smoothing with a smoothing factor equal to 0.05. It can be seen how with this type of smoothing, the general trend of the PLE is well tracked without introducing the contribution of small variations.

4.2 PLE for unfiltered and filtered signals

Once the general trend of the PLE in the single channel CZ was verified, a 5x5 mask around CZ was created. All PLE values for each of the channels adjacent to CZ within the area defined by the mask were calculated. The Fig. 4.2 aims to highlight a uniform trend of the PLE in the channels surrounding CZ, thus allowing for a consolidated analysis of CZ rather than across all the channels. The Fig.4.2 shows the trends of the PLE in the different channels, both with and without their mean. Subtracting the mean from the signal results in a shift of the signal to zero. Once all the signals have zero mean, a common trend of the PLE across the channels can be visually appreciated.

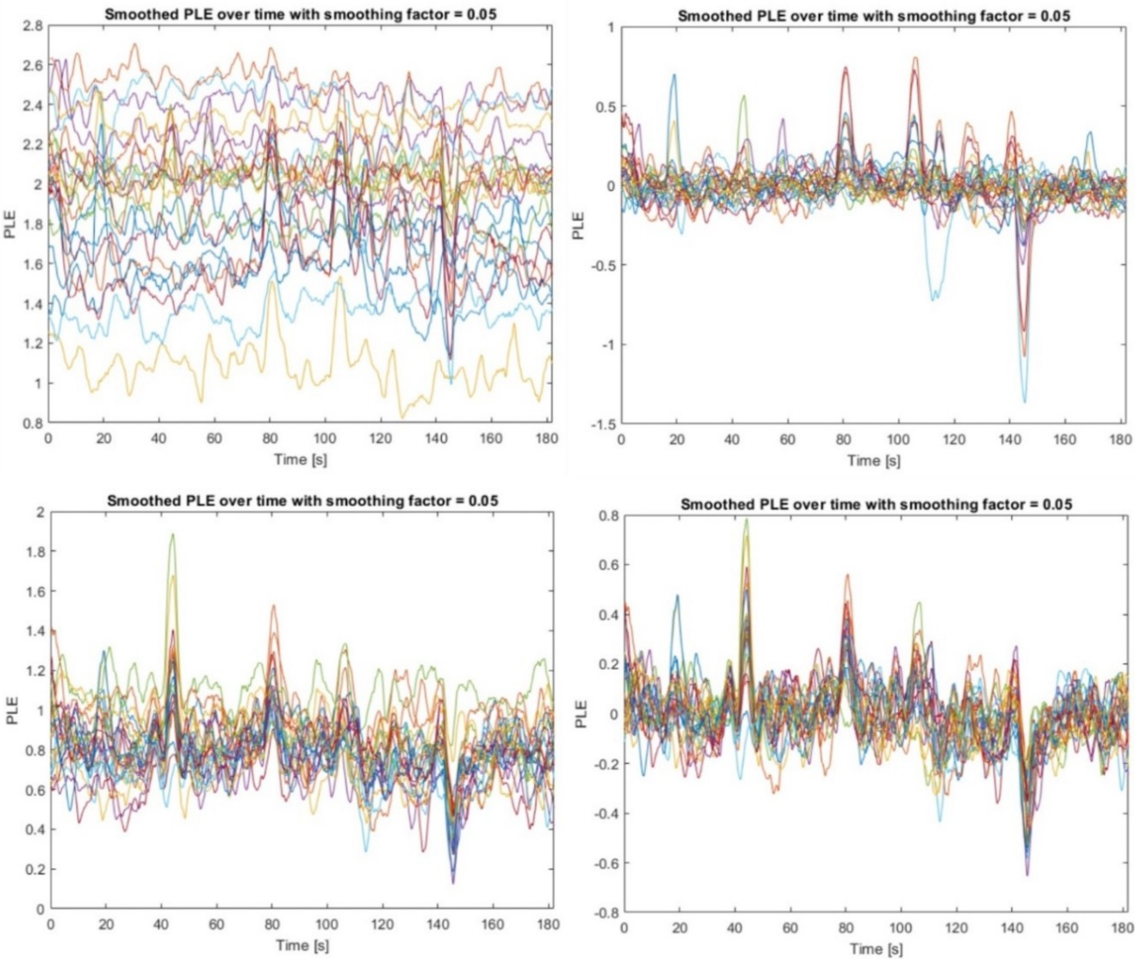

Fig. 4.2: Trend of the PLE across all channels adjacent to CZ within the specified mask and PLE trend without averaging of all channels adjacent to CZ to better visualize the general trend of the PLE in the different channels without the shift due to the channel averaging. The first column represents the PLE signals of the channels around CZ in the case of filtered and unfiltered signals without the average shift. In the second column instead, the average has been removed from the signals. This graph shows the data of the fifth subject.

In Fig. 4.2 it is possible to observe how the PLE trend varies before and after filtering. The values assumed before filtering are different for each channel with well-marked shifts along the vertical axis probably due to some artifacts present. After filtering the signal, the channel values settle around an average value and reflect a similar trend. This suggests that the PLE is redundant in the various channels and that it has lower values than those highlighted without filtering. It is also interesting to note that before and after the filtering phase, PLE has maintained the same trend over time.

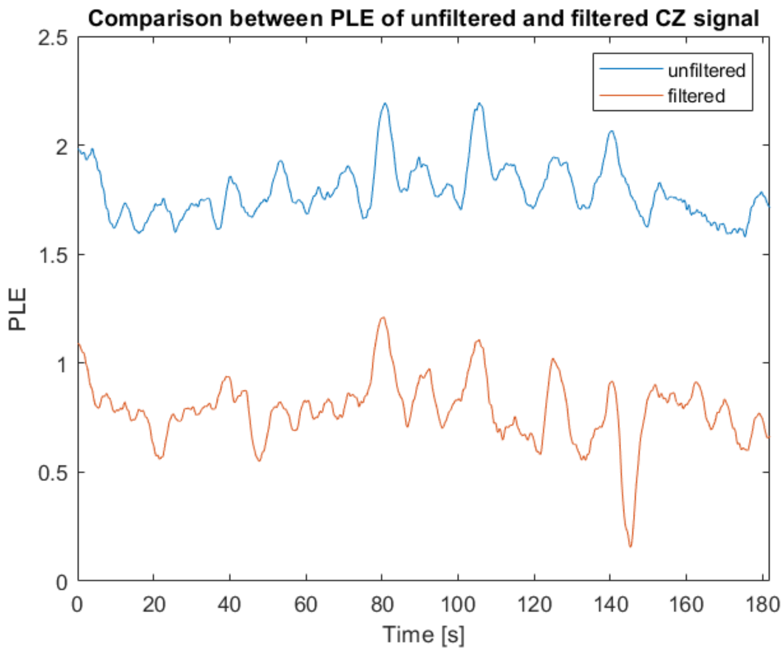

Fig. 4.3: Representation of a portion of PLE signal in time from the CZ channel of the fifth subject. In blue is shown the PLE signal calculated on the unfiltered signal and in red is shown the PLE signal calculated on the filtered signal.

From Fig. 4.3 it can be seen how the signal's trend over time maintains the same properties for the filtered and unfiltered signal. This implies that the application of filtering has no drastic effects on the general PLE trend but still manages to capture more the trend of the frequency bands. In addition, it is possible to notice the shift between the filtered and unfiltered signal due to low frequencies that distort the actual PLE values.

4.3 Correlation between EOG and unfiltered and filtered EEG signals

After the visualization phase, the correlation between the signals in the prefrontal and frontal area of the scalp of the subjects with EOG was calculated. This practice was used to have more information on the quality of the signals extracted in real time compared to those used during the offline analysis after filtering. The averages of the Pearson correlation coefficients of the prefrontal signals before and after filtering in the three phases of the protocol are reported in Table 4.1.

	Subj 1	Subj 2	Subj 3	Subj 4	Subj 5
$r_{1^{st}\ phase\ before\ filtering}$	0.078803	0.019342	0.13384	0.10074	0.42968
$r_{2^{nd}\ phase\ before\ filtering}$	0.29206	0.054058	0.18906	0.13172	0.21053
$r_{3^{rd}\ phase\ before\ filtering}$	0.26655	0.082772	0.10074	0.10598	0.18764
$r_{1^{st}\ phase\ after\ filtering}$	0.067159	0.04444	0.082954	0.047379	0.16159
$r_{2^{nd}\ phase\ after\ filtering}$	0.095996	0.052537	0.11491	0.081431	0.060711
$r_{3^{rd}\ phase\ after\ filtering}$	0.076235	0.047522	0.038108	0.066911	0.10943

Table 4.1: Average of the Pearson correlation coefficient (r) values calculated between the EOG and the EEG signals measured in the prefrontal and frontal regions.

From Table 4.1 it can be seen that for the unfiltered signals there is a good correlation between the EOG signal and the signals in the frontal areas. In particular, it must be noted that the values presented derive from the average of the correlation coefficients of the different channels so there are channels that have even greater correlation with the EOG signal. It can be appreciated that in all cases the average correlation coefficient has decreased suggesting a good cleaning of the EOG from the EEG signals.

4.4 Correlation between PLE in CZ and PLE of all adjacent channels

To obtain a quantitative measure of the conformity of the PLE trend in the CZ channel compared to the adjacent channels, the average PLE signal of the channels within the mask was calculated. Once the average PLE signal of the nearby channels was computed, the Pearson correlation coefficient between this signal and the PLE of the CZ channel was determined. The aim is to understand the correlation between the trend of the PLE in CZ, the channel whose PLE value is used to produce the noise, and the channels adjacent to CZ.

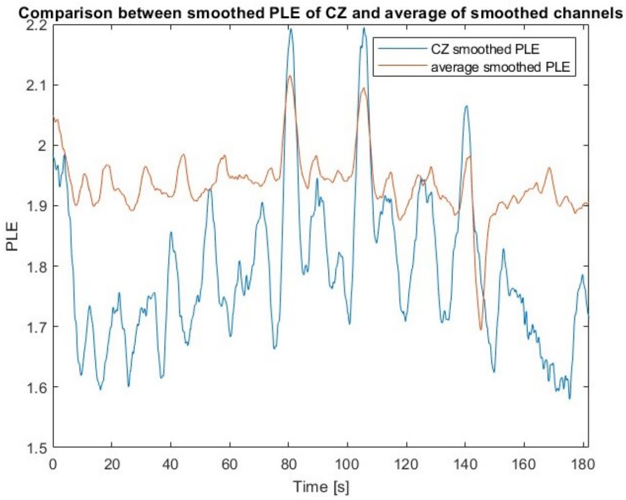

Fig. 4.4: Trend of PLE in CZ compared to the trend of the overall average PLE in the channels adjacent to CZ. This graph shows the data of the fifth subject.

In Table 4.2, the Pearson correlation coefficients, calculated for the different subjects in the three phases of the protocol, have been shown.

	Subj 1	Subj 2	Subj 3	Subj 4	Subj 5
$r_{1^{st}\ phase\ before\ filtering}$	0.48529	0.18564	0.80525	0.76733	0.55975
$r_{1^{st}\ phase\ after\ filtering}$	0.63858	0.58585	0.43664	0.67073	0.4875
$r_{2^{nd}\ phase\ before\ filtering}$	0.16829	0.17579	0.61217	0.68813	0.37265
$r_{2^{nd}\ phase\ after\ filtering}$	0.69939	0.60962	0.18071	0.91211	0.73535
$r_{3^{rd}\ phase\ before\ filtering}$	0.36984	0.26794	0.17267	0.67691	0.37748
$r_{3^{rd}\ phase\ after\ filtering}$	0.8853	0.64189	0.67073	0.67227	0.49174

Table 4.2: Pearson correlation coefficients (r) for the 5 subjects in the three steps of the protocol for unfiltered and filtered signals.

Table 4.2 shows the correlation values between the PLE in the CZ channel and the mean PLE value in the channels adjacent to CZ within the mask. The results for unfiltered signals show that there is no consistent general trend between CZ PLE and average signals. The correlation coefficients presented cover a too wide range of values. The causes of this trend could be due to the amount of noise present on the different channels. The second subject, for example, had a substantial mass of hair which may have resulted in distortion and artifacts between the signals adjacent to CZ leading to different changes in the recording of brain signals. The high correlations may be due to a general trend, but it may also be due to a common channel artifact. Muscle movements or eye movements are not eliminated in this phase of the experiment and therefore high correlations can also be due to signals with a high presence of artifacts. The only trend seen in this table is a decrease in signal correlation from the first phase of the protocol to the two following. The values of the correlations in the second and third phases tend to decrease for all subjects presented except for the second subject, which is considered as the noisiest and less accurate. At this stage of the analysis, it is not possible to draw conclusions about the correlation of the PLE trend around CZ. However, the values presented in the table show a correlation, often high, especially in the first phase of the protocol, between CZ and the average of the channels around CZ. However, greater conclusions can be drawn regarding the correlation with the filtered signals. For the first, second, fourth and fifth subjects there was a substantial increase in the correlation between the average PLE of neighbouring channels and the PLE in CZ. This provides even greater support for the hypothesis that there is a consistent pattern between the channels in the central area of the head and CZ. In the relation to the third subject, which showed the highest correlation in the analysis without filtering the signals, a decrease is noted in the first two phases of the experiment where there was a high correlation.

This variation could be due to inadequate signal filtering which led to a mismatch between the different PLE signals in the different channels around CZ. The high correlations present in the analysis without filtering could be due to some artifacts present in most channels. Considering that the recording in CZ was made because the channel CZ is usually the one exposed to less contamination of artifacts and noise, it is noticed that with a greater cleaning of the signal the general trend around that channel turns out to be more uniform.

4.5 Comparison between complexity metrics and PLE

After comparing the average values of PLE and PLE of channel CZ, graphs were extracted for complexity metrics compared to PLE. All the complexity indices have been calculated over time to provide signals that can be compared with PLE. The data were normalised for comparison. The signals of the different complexity metrics compared with the subject's PLE are then inserted into the same graph. The complexity metrics used are: Spectral Entropy, Spectral Asymmetry Index, Relative Power and Band Power Ratios. This stage of the analysis serves to have a deeper understanding of the meaning of PLE. By comparing the PLE trend with the complexity metric trend, it is possible to understand how the PLE trend has evolved in general and in individual frequency bands.

4.5.1 Spectral Entropy

The first measure of calculated complexity is Spectral Entropy.

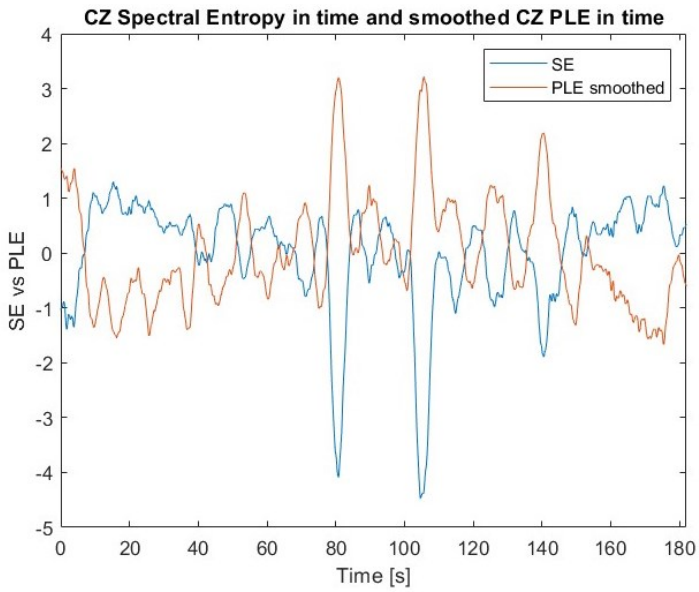

Fig. 4.5: Comparison between SE and PLE over time of channel CZ. This graph shows the data of the fifth subject.

From Fig. 4.5 it can be seen how the two graphs are exactly mirrored along the horizontal axis. With the increase of PLE there is a proportional reduction of SE and vice versa. This behaviour is due to the significance of the two metrics. The SE measures the disorder or complexity of the frequency content of a signal. Higher SE indicates a more complex sample distribution and therefore lower concentration of the PSD in the different frequency bands. A lower SE indicates that the data is more concentrated in a given frequency range. A high SE indicates a wider frequency distribution, while a low SE indicates a higher concentration at certain frequencies. The relationship we expect is therefore of inverse proportionality [6]. A high SE implies that the distribution in the frequency bands is more dispersed, the signal has a wide frequency range and decays more slowly. This corresponds to a lower PLE. In fact, a lower slope of the PSD regression line implies a more even distribution of the PSD in frequency bands and a higher content at high frequencies. A high PLE corresponds to a lower SE. This behaviour is due to the fact that a higher frequency makes the angular coefficient of the regression line greater, and a faster decay of the PSD implies a higher concentration of the energy of the signal at lower frequencies.

4.5.2 Spectral Asymmetry Index

The second complexity metric used for the analysis is the Spectral Asymmetry Index. Fig. 4.6 shows the performance of PLE and SASI of the fifth subject's CZ channel during the first phase of the protocol.

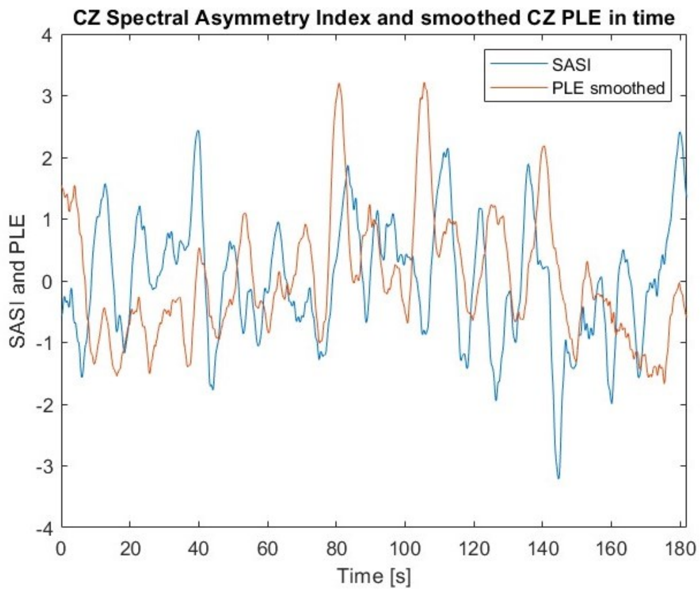

Fig. 4.6: This image shows the trend of PLE and SASI of the fifth subject's CZ channel during the first phase of the protocol.

The SASI quantifies the asymmetry in the signal spectrum and is calculated by comparing high and low frequencies to reveal which part dominates the spectrum. Positive values indicate a higher presence of power at low frequencies of the signal while negative values indicate a predominance of high frequencies. In Fig 4.6 is shown how similar the trends are. This behaviour is due to the fact that the PLE increases when there is an increase in signal strength at low frequencies or a decrease in power at high frequencies. The SASI behaves similarly to the PLE since an increase in power of the low frequencies makes the coefficient of asymmetry greater. The same reasoning, but in reverse, can be made for high frequencies. Usually, a larger range is taken for high frequencies when computing the SASI. This allows to have a sum of the powers of high frequencies that is comparable to the sum of the powers at lower frequencies. In our case the maximum assumed frequency is 40 Hz and therefore the powers at lower frequencies will have a greater contribution in the calculation of the asymmetry index. In conclusion, PLE and SASI show a positive relationship while showing slightly different signal strength trends. The SASI, in fact, highlights the dominance of high frequencies over low ones while the PLE expresses the power decay rate by describing the general structure of the signal in frequency. The SASI also gives us information on the dominance of certain frequencies, while the PLE gives us information on how gently or sharply the dominance changes.

4.5.3 Relative Power

The third complexity index compared with PLE is Relative Power. The following are the graphs of the PLE and RP performance for the different frequency bands of the fifth subject's CZ channel during the first phase of the protocol. The RP measures power in a specific frequency band in relation to total signal power in the frequency range considered. The relative power is calculated for each frequency band to provide information on the dominance and pattern of brain oscillations.

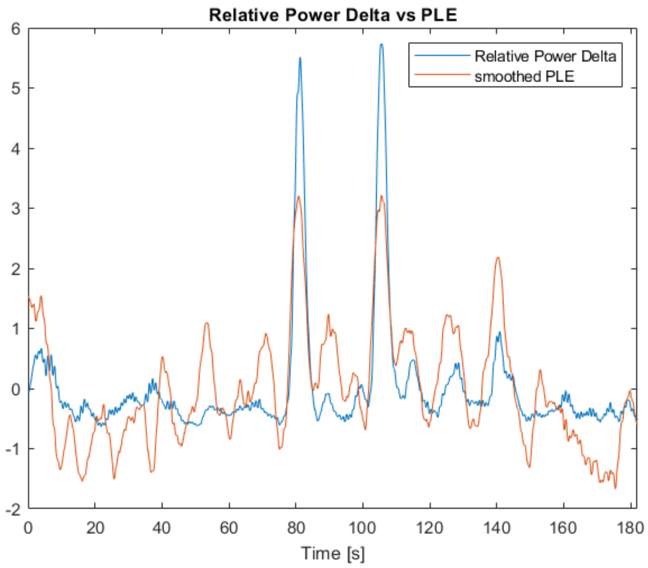

Fig. 4.7: Delta band RP trend [0.5 - 4 Hz] compared to the PLE trend over time. This graph shows the data of the fifth subject.

From Fig. 4.7 it can be seen a direct proportionality between the RP of the Delta band and the PLE. In this case, it is comparing how the power at lower frequencies is related to the overall power decay rate on all frequencies. A high PLE indicates that the power decreases rapidly with increasing frequency, which means that the power is concentrated at low frequencies. This corresponds to a higher relative power in the Delta band. Decreases in PLE suggest a flatter course of the power spectrum and thus a decrease in low frequencies. The general trend shown in the figure represents a positive association between PLE and RP in Delta band. However, there are inconsistencies in certain time zones. In fact, from 15 to 40 seconds it can be noticed that there is no actual change of the RP, but there is a change in the PLE. The same pattern can be seen from 160 seconds until the end of the recording. This trend can be explained by the fact that there is no predominance of Delta waves as shown by the RP values, but other frequencies are varying. Power variations in the higher frequency bands induce a decrease in PLE values, leading to a different trend between RP and PLE. This result highlights that there is a predominance of the Delta power during the calculation of the PLE but also shows that the PLE not only captures the contribution of the frequency band with higher content but also manages to capture the other variations in the higher frequencies.

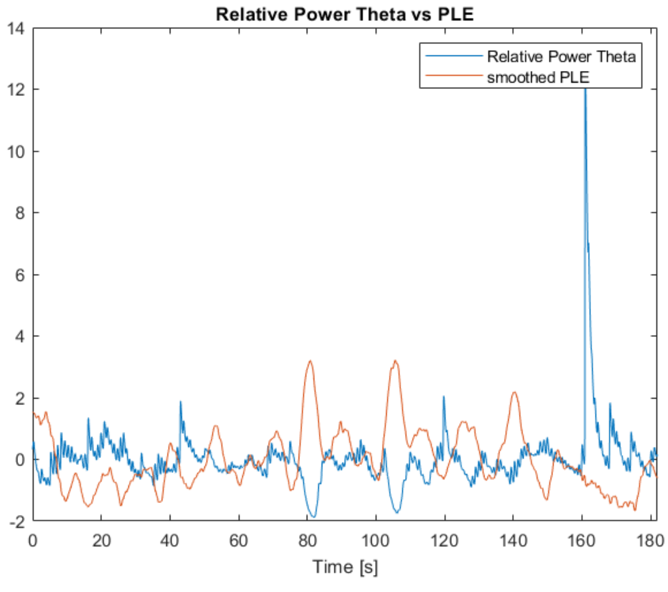

Fig. 4.8: Theta band RP trend [4 - 8 Hz] compared to the PLE trend over time. This graph shows the data of the fifth subject.

From Fig. 4.8 it can be observed an almost opposite trend between the RP in the Theta band and the PLE. This is due to the fact that in low-processed signals, and with noise and artifacts, the signal strength is much higher in Delta band. Theta band RP does not show the expected pattern which is usually similar to the Delta band RP pattern. In fact, an increase in power in the Theta band is expected to be matched by an increase in PLE. The graph shows a different trend between the two metrics, although they behave similarly in some time periods. The PLE does not seem to be much affected by this band except in transition zones. The fact that theta waves do not visually affect the PLE may be due to the fact that they do not cover a high frequency range, and the contribution is therefore not captured properly. [7]

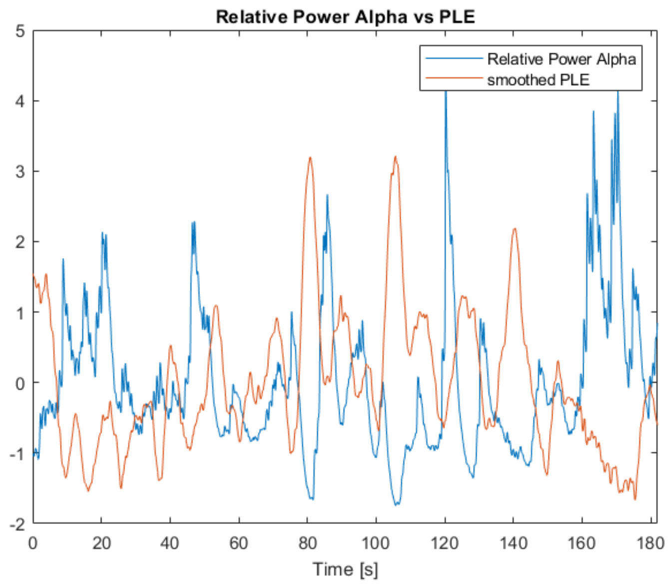

Fig. 4.9: Alpha band RP trend [8 - 13 Hz] compared to the PLE trend over time. This graph shows the data of the fifth subject.

From Fig. 4.9, we can see a discordant trend between the RP in Alpha band and the PLE. In fact, the increase of the first one is a decrease of the second and vice versa. In general, this inverse relationship between the two measurements is evident since an increase in the Alpha band causes a decrease of the angular coefficient of the regression line and therefore also a decrease of the PLE. An increase in power in the Alpha band, therefore, causes the slope of the power decay to be reduced, thus lowering the PLE. In some areas of the graph, it can be seen overlaps in the trend of the two signals especially for small periods of time. This is due to the fact that alpha band RP and PLE show temporal variability with fluctuations on different time scales. The RP, in fact, varies more quickly from one temporal instant to another since it identifies the power variation of a single frequency band. Therefore, a sudden change in the Alpha band is not associated with such a rapid variation of the PLE since, identifying the general trend of the spectrum, it has longer variation times. The fact that there is no strict correlation between the RP of the Alpha band and PLE allows the two values to be used in the future to modify certain parameters of the sound produced. For example, the Alpha band value could be used to adjust the sound volume proportionally. By increasing the volume of the sound, following the trend of the Alpha band, we will also increase the evoked response in the subject, bringing him back to a state of heightened attention.

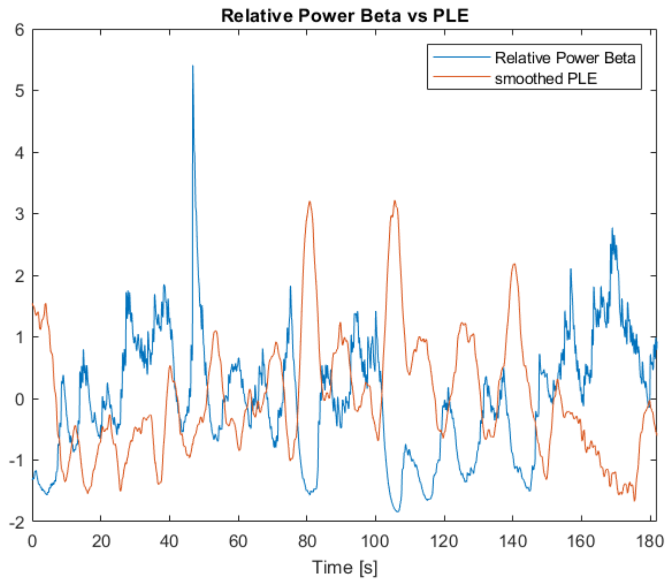

Fig. 4.10: Beta band RP trend [13 - 30 Hz] compared to the PLE trend over time. This graph shows the data of the fifth subject.

In Fig. 4.10, it can be seen an opposite trend between the RP in Beta band and the PLE. This trend is expected because positive variations in power in the Beta band correspond to a decrease in PLE and vice versa. In Fig. 4.10 it can be seen the specularity of the trend of the two metrics, with respect to the horizontal axis. This is because, among all the bands, the Beta band is the one that covers the greatest number of frequencies. A variation of the power in this band, therefore, leads to an increase or decrease in the RP, opposite to the PLE. However, some areas of the graph show divergent trends that could be due to decreasing or increasing power in other frequency bands.

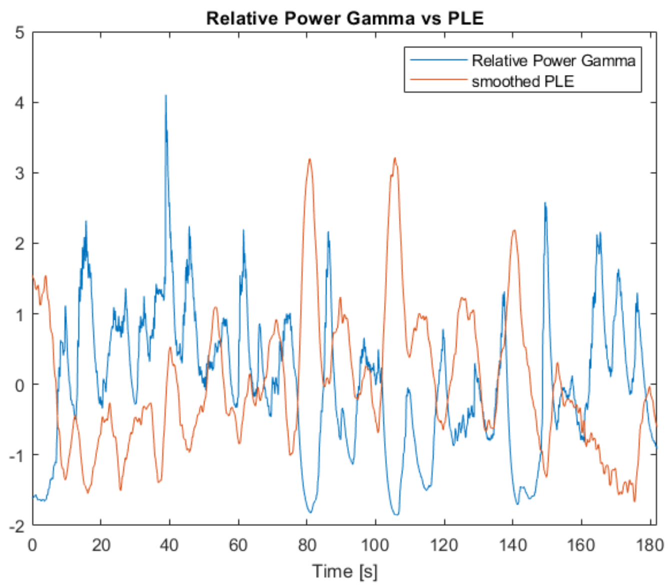

Fig. 4.11: RP trend of the Gamma band [30 - 40 Hz] compared with the PLE trend over time. This graph shows the data of the fifth subject.

The Fig. 4.11 shows a trend with inverse proportionality between the two measures. In fact, as the PLE increases there is a decrease in the Gamma band. An increase in power in the Gamma band is often associated with a decrease in PLE. The peak present at about 40 seconds could be due to rapid power fluctuations in the Gamma band which often reflect immediate neural processing demands and result in rapid and pronounced changes in the signal.

4.5.4 Band Power Ratios

The latest complexity metric compared to PLE is Band Power Ratios. The relationships considered were the relationships between the Theta band and the Alpha band, between the Theta band and the Beta band, between the Delta band and the Alpha band and between the Delta band and the Beta band.

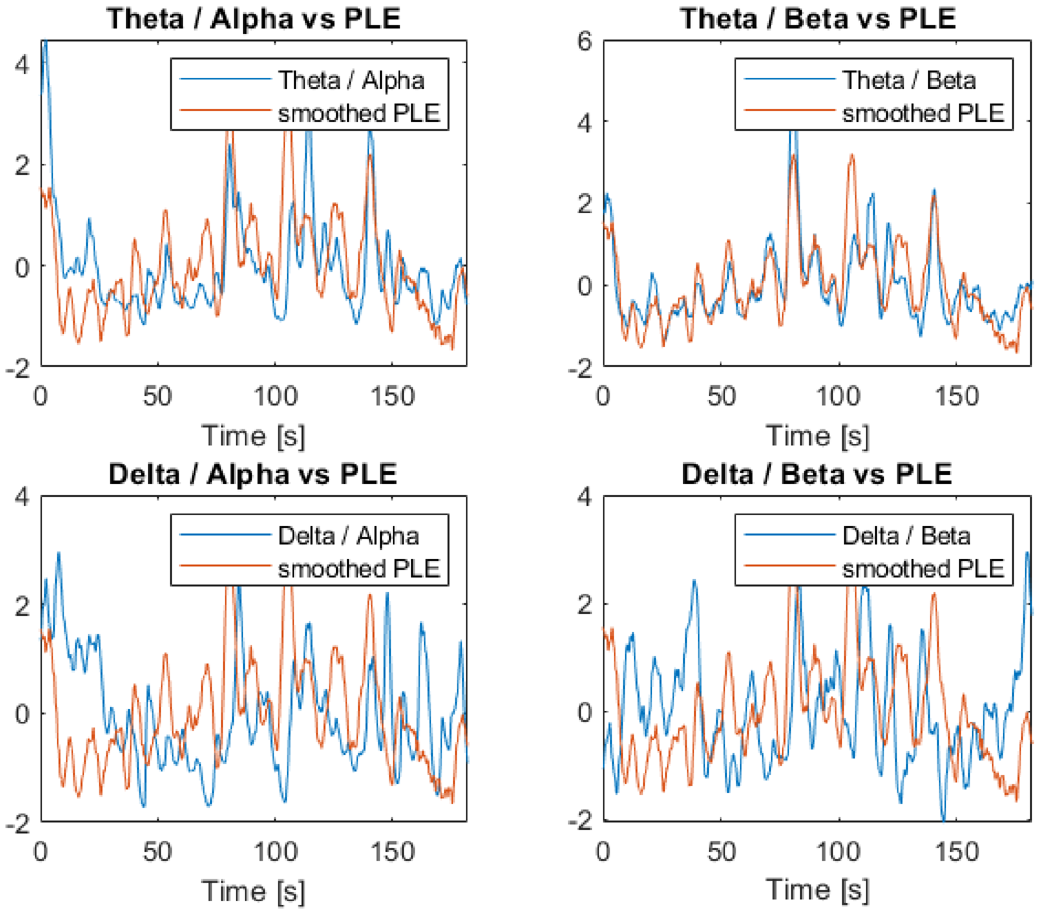

Fig. 4.12: Relationships between power bands ratios and PLE. This graph shows the data of the fifth subject.

The Fig.4.12 represents the time trend of the above-mentioned BPR. From Fig. 4.12 it can be seen that an increase in PLE may coincide with higher theta-alpha and delta-alpha ratios indicating also states of relaxation. The Fig.4.12 shows a trend in the ratio between the Theta and Beta bands very similar to the trend of PLE [15]. This may indicate that the overall trend could be described by this ratio. In fact, the Theta band and the Beta band are the bands with the largest frequency ranges and therefore they cover a wider signal spectrum. It can be seen that the relationship between the Delta band and the other two frequency bands is more interesting. In fact, if you take the first 50 seconds of the signal you can appreciate how there is a difference between the activity of the PLE and the BPR. This is due to the contribution of Alpha compared to Delta. In fact, in the Fig. 4.7 and in Fig 4.9 it can be seen how Delta follows the precise trend of the PLE while Alpha almost the opposite. The inverse behaviour of power in the Alpha band makes the two trends differ. This is also the case with the Beta band. This is not the case with the Theta band ratios because the RP graphs showed a strangely similar trend between the two metrics and therefore a direct proportionality relationship. This implies that when one power increases the other also does not lead to variations in their ratio [37].

4.5.5 Correlation between PLE and complexity measures

After visual analysis, the correlation between PLE and complexity measures in the CZ channel was calculated for the five different subjects. Table 4.3 shows the correlation values for the analysis with unfiltered signals and Table 4.4 the correlation values for the analysis with filtered signals.

	Subj. 1	Subj. 2	Subj. 3	Subj. 4	Subj. 5
r_{SE-PLE}	-0.48	0.14	-0.57	-0.27	-0.85
$r_{SASI-PLE}$	0.22	-0.50	0.71	0.61	0.19
$r_{\frac{Theta}{Alpha}-PLE}$	0.32	0.42	0.39	0.22	0.42
$r_{\frac{Theta}{Beta}-PLE}$	0.58	0.83	0.74	0.73	0.72
$r_{\frac{Delta}{Alpha}-PLE}$	-0.11	-0.60	0.36	-0.17	-0.05
$r_{\frac{Delta}{Beta}-PLE}$	0.16	-0.41	0.77	0.48	0.08
$r_{\frac{Alpha}{Beta}-PLE}$	0.22	0.44	0.45	0.48	0.003
$r_{DeltaRP-PLE}$	0.42	0.78	0.05	0.29	0.67
$r_{ThetaRP-PLE}$	-0.32	-0.70	-0.02	-0.20	-0.39
$r_{AlphaRP-PLE}$	-0.26	-0.59	-0.04	-0.22	-0.42
$r_{BetaRP-PLE}$	-0.37	-0.59	-0.08	-0.15	-0.53
$r_{GammaRP-PLE}$	-0.25	-0.51	-0.04	-0.18	-0.49

Table 4.3: Representation of the Pearson correlation coefficients (r) between the PLE and the complexity metrics derived from the unfiltered CZ channel signal. The value in each box indicates the average value of the correlation in the three different phases of the experiment for a single subject.

	Subj. 1	Subj. 2	Subj. 3	Subj. 4	Subj. 5
r_{SE-PLE}	-0.25	-0.74	-0.51	-0.46	-0.90
$r_{SASI-PLE}$	0.85	0.87	0.88	0.87	0.84
$r_{\frac{Theta}{Alpha}-PLE}$	0.30	0.43	0.36	0.29	0.46
$r_{\frac{Theta}{Beta}-PLE}$	0.54	0.80	0.63	0.73	0.69
$r_{\frac{Delta}{Alpha}-PLE}$	0.54	0.73	0.60	0.41	0.64
$r_{\frac{Delta}{Beta}-PLE}$	0.73	0.86	0.78	0.74	0.77
$r_{\frac{Alpha}{Beta}-PLE}$	0.22	0.48	0.44	0.54	0.01
$r_{DeltaRP-PLE}$	-0.31	-0.23	-0.11	-0.10	-0.17
$r_{ThetaRP-PLE}$	-0.25	-0.07	0.01	-0.07	-0.10
$r_{AlphaRP-PLE}$	0.13	0.20	0.06	0.06	0.24
$r_{BetaRP-PLE}$	0.21	0.06	0.01	0.07	-0.05
$r_{GammaRP-PLE}$	0.29	0.11	0.16	0.07	-0.14

Table 4.4: Representation of the Pearson correlation coefficients (r) between the PLE and the complexity metrics derived from the filtered CZ channel signal. The value in each box indicates the average value of the correlation in the three different phases of the experiment for a single subject.

Comparing Table 4.3 and Table 4.4, it can be seen that the filtering make she values more uniform between the different subjects. As noted above, during the analysis by visual inspection of the complexity measures, there is a close correlation between PLE performance and SE. In fact, the values reported in Table 4.3 and Table 4.4 show an inverse correlation between the two metrics, confirming what has been shown. The correlation values with SASI indicate a close proportionality with PLE. This is an expected result as an increase in power in the higher frequency bands corresponds to an increase in PLE and vice versa. The same reasoning can be extended to a decrease in SASI. The values between the Theta-Beta power ratio and PLE show a high correlation, probably due to the fact that Theta-band and Beta-band cover a greater frequency range of the spectrum. The values of Delta-Beta power ratio and PLE also show a very high correlation. This is especially evident for the analysis of filtered signals. As far as the values between the Alpha-Beta power ratio and PLE are concerned, no great differences emerge between the calculation in filtered and unfiltered signals. This is an indication of correctly executed filtering that did not change the components of the intermediate frequencies. What is most surprising are the results of the correlation between RP and PLE. In fact, the values before and after filtering are almost inverse. The values of the RPs are most influenced by the total signal power, which, before filtering, was focused on the Delta band. However, the correlations between RPs and PLE are very low, indicating that PLE does not only capture the trend of one frequency band but rather the trend of the entire frequency spectrum. Analysing the second subject, the one considered to be the noisiest, it emerges that filtering led to results in line with those of the other subjects. In the results in Table 4.3, the second subject shows contrasting metrics, especially for SE and SASI values, which are the two indices least affected by inter-subject variations. Filtering also yielded very good results for the second subject as shown in Table 4.4. In general, after filtering, the metrics that show the most positive correlation are SASI, the Theta-Alpha power ratio, the Delta-Alpha power ratio and the Delta-Beta power ratio. The metric that, before and after filtering, shows the greatest negative correlation is SE.

4.6 Linear Trend

Another analysis which was carried out on the PLE signal was to calculate the linear regression line. This analysis was made to see if there was a general trend of PLE over time. For example, through this analysis it could be understood whether there was a decrease or an increase of the systematic PLE over time. As shown in Fig. 4.13 for the fifth subject, no trend deviating from the linear trend was observed. The trend of PLE was found to be subjective. In fact, in some subjects it was observed that the trend between the different phases could be linear or increasing or decreasing without a common pattern among the subjects. Fig. 4.13 shows a decrease in the mean of PLE signals over time calculated from filtered signals. In these, the PLE values are much lower than those calculated with raw signals. This lowering was found to be common to all subjects.

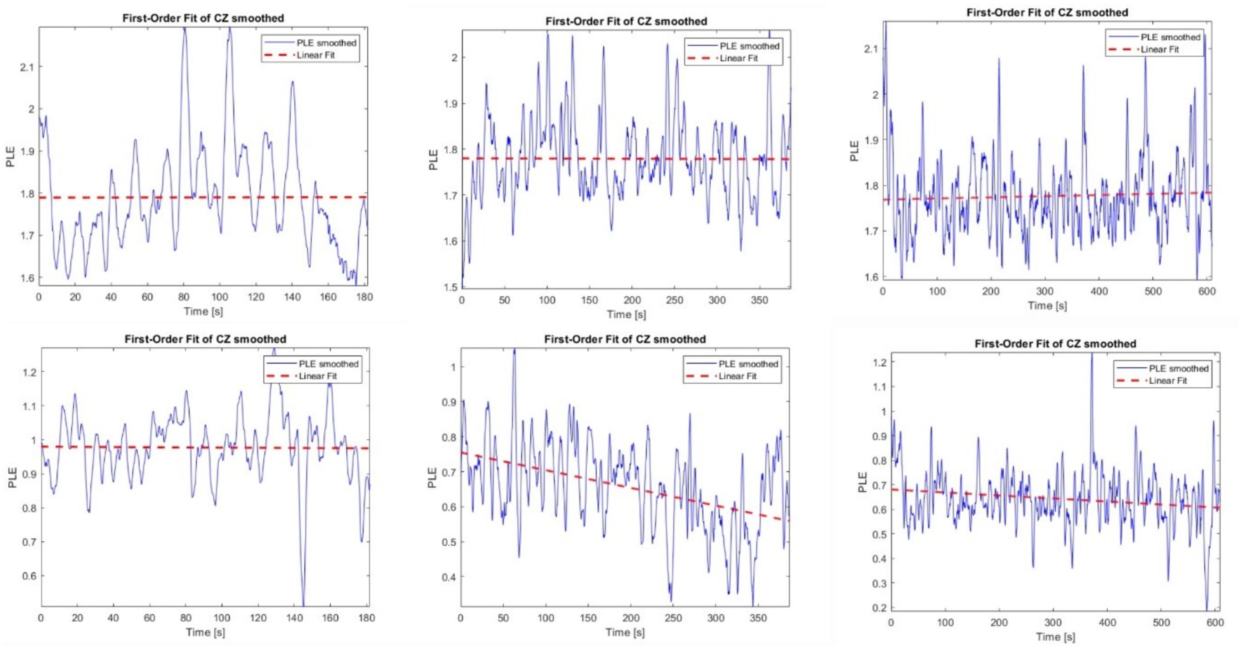

Fig. 4.13: Linear trend of PLE through the different phases of the protocol. The images in the first row are derived from the calculation of PLE with the unfiltered signals, while the images in the second row are derived from the filtered signals. Along the columns are the three phases of the protocol. This graph shows the data of the fifth subject.

4.7 Topographic Maps

After investigating the different complexity metrics, topographic maps were extracted. The first extrapolated maps identify the average PLE for each channel adjacent to CZ. The mean of the channel is used because, as previously stated, it was noted that the trend of PLE in all channels and for all subjects of the experiment over the observation and recording time is linear. Then the mean of the channels was taken to verify if there was an intrasubject or intersubject consistency between the different brain areas.

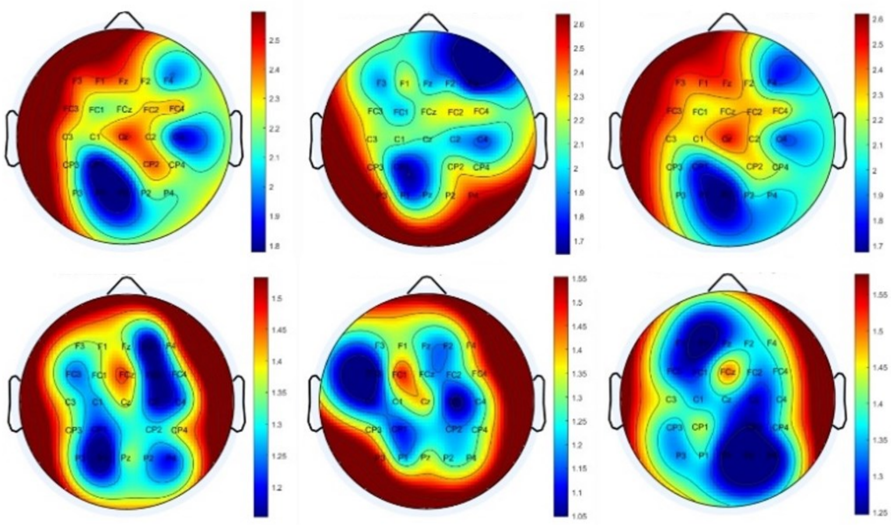

Fig. 4.14: Topographic maps of the mean PLE of the channels adjacent to CZ of the fifth subject. On the first line we find PLE data calculated from unfiltered signals while in the second line there are PLE data calculated from filtered signals. The three phases of the experiment are presented along the columns.

From Fig. 4.14, it can be seen that there is a strong consistency between the different areas around CZ when analysing with unfiltered signals. In fact, a common activity can be observed in all three phases of the experiment. In the analyses with the filtered signals, on the other hand, the consistency between the different experiments is less, but consistent patterns can still be recognised. If, with the unfiltered signals, the result is very similar between the different phases of the protocol, with the filtered signals it is less evident that there are similar patterns between the different phases. In the central frontal zone, in fact, a higher average can be observed. Similar trends can also be observed in the centre-left and centre-right areas. In this case the consistency between the PLE trends of the areas adjacent to CZ in the first line of Fig 4.14 could be due to the presence of artifacts consisting in the channels occurring in all three phases. The filtering applied may cause small variations in the output of the results due to the type of filtering applied. In the analysis with filtered signals, adaptive thresholds are used to select the independent components to be removed. It is therefore possible that more components were taken depending on the amount of correlation between the independent components and the EOG. In any case, similar patterns can be observed both in the analysis with unfiltered signals and in that with filtered signals. After calculating the average PLE for the area surrounding CZ, the PLE trend, in the different brain areas, was analysed. First of all, the PLE over time was calculated for each channel and averaged. The brain areas were divided into region of interests (ROIs): prefrontal area, frontal area, temporal area, central area, parietal area and occipital area. The average PLE value of the channel that fell within a certain ROI was averaged with the other channels belonging to that ROI. In this way, a map was obtained for each subject showing the average PLE value in the different brain areas. This allows to compare the average PLE patterns in different brain regions among subjects to investigate a possible intersubject pattern.

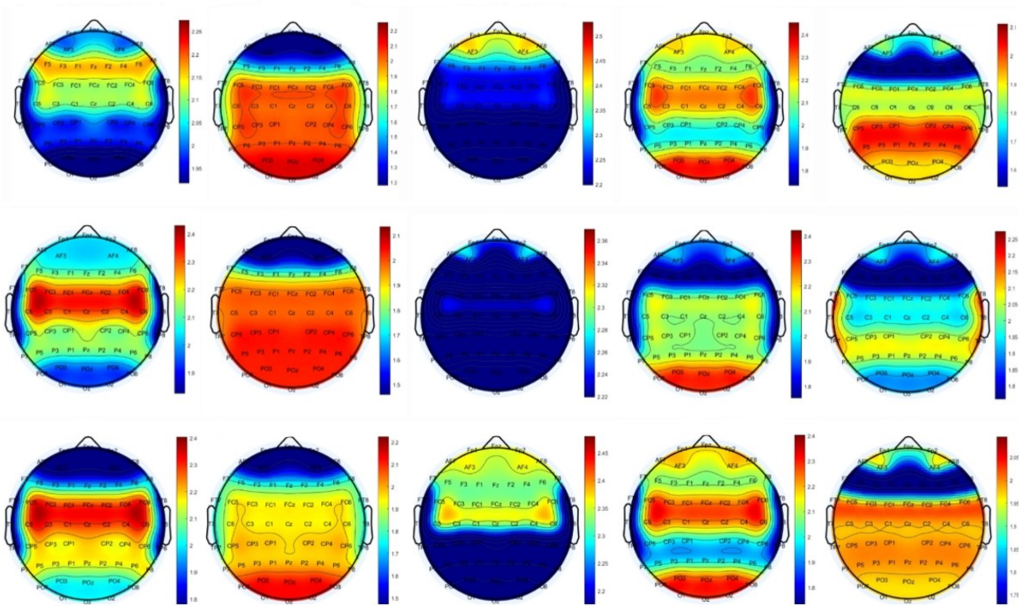

Fig. 4.15: Topographical maps of the mean in the regions of interest (ROI) for each subject during the protocol. Along the columns are arranged the subjects (five columns and five subjects) while along the rows there are the three phases of the protocol (three lines and three phases). The signals used to create these charts have not been filtered.

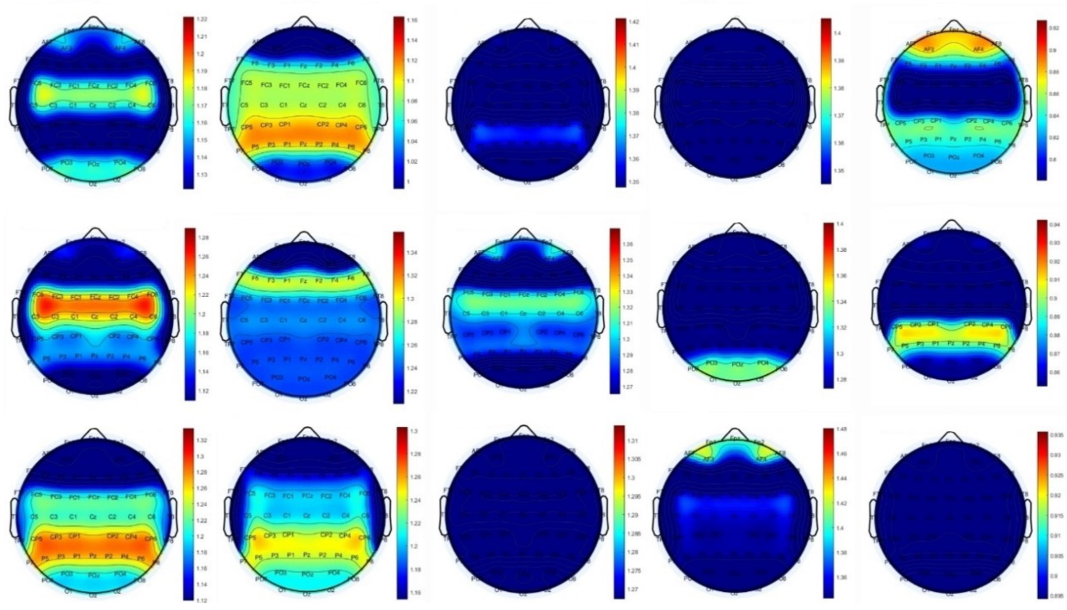

Fig. 4.16: Topographical maps of the mean in the regions of interest (ROI) for each subject during the protocol. Along the columns are arranged the subjects (five columns and five subjects) while along the rows there are the three phases of the protocol (three lines and three phases). The signals used to create these charts have been filtered.

In Fig. 4.15 is shown the average PLE of the five subjects in the three phases of the protocol. There is a big difference in the intensity of the maps and therefore the averages between the topographical maps calculated with filtered signals and those calculated with unfiltered signals. In general, all unfiltered signals have a higher PLE trend. The topographic maps show two different PLE trends. However, both for the filtered and unfiltered signals it can be appreciated that there is no variation of PLE between the different phases of the protocol. Some considerations can be made about the topographical maps extracted from the filtered signals, which are those that most closely mimic the real trend of the PLE. All subjects show different trends but not entirely contrasting. From the images you can see that there is a similar trend in all subjects in the frontal area. The PLE, in fact, in this area seems to be low in all subjects except for the first subject in the second phase of the experiment. The same pattern can be seen in the temporal areas of the subjects. In the central areas, there was a drop from the first to the third task in the second, third and fourth subjects. The variation is gradual and can be appreciated as the PLE in the central area decays. The occipital zone remains active and above average in the third, fourth and fifth subjects while it lowers in the first and second subjects.

4.8 Sound Generation

Finally, the spectrogram of the generated sound was observed, showing the trend of the frequency spectrum over time.

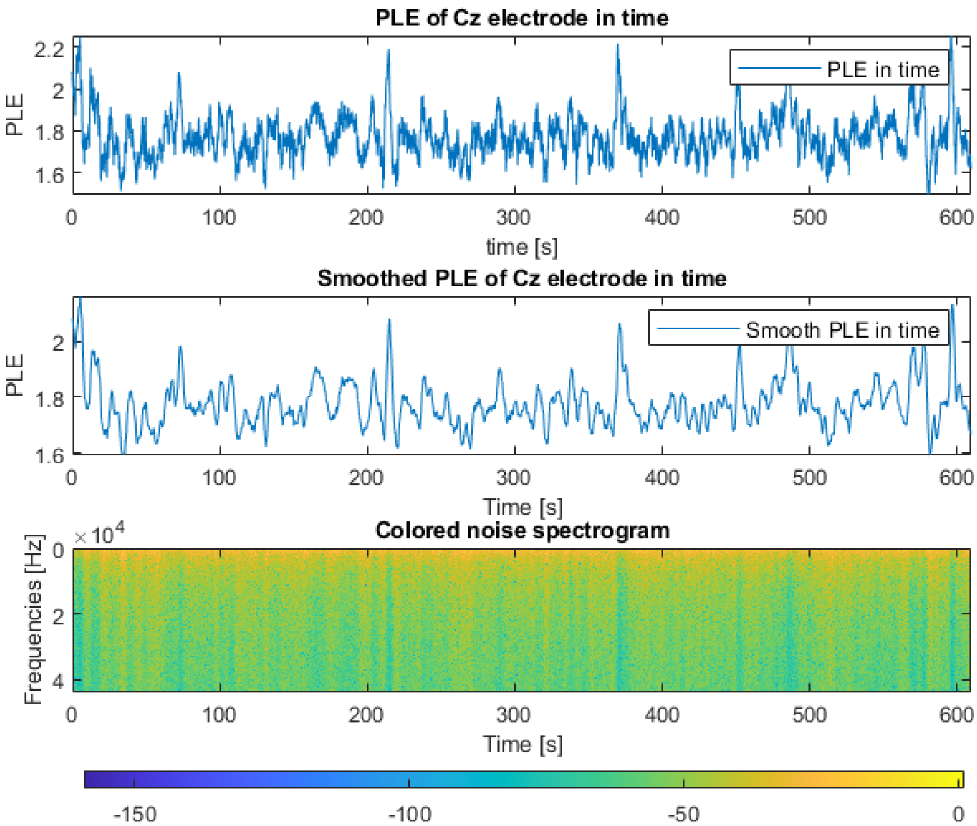

Fig. 4.17: The time-course of the PLE in rough, the time-course of the smoothed PLE and the spectrogram of the generated sound.

Fig. 4.17 shows that the sound generated is perfectly proportional to the value of the PLE. In fact, with an increase in the value of the PLE there is a sudden decrease in the frequency spectrum. This follows the desired trend since, according to the power law, a higher value of the exponent, in our case the PLE, corresponds to a decrease in the scale factor. The scale factor causes the high frequencies of the noise to decay faster. If you have lower PLE values the frequency spectrum will decay more slowly. This trend can be observed very well in Fig. 4.17 where, around 220 seconds and around 375 seconds of recording, PLE peaks occur.

4.9 Mean and Standard Deviation before and after filtering

For further analysis, the mean and standard deviation of PLE signals in the CZ channel were also calculated to try to identify an intra-subject and inter-subject trend.

	Subj 1	Subj 2	Subj 3	Subj 4	Subj 5
$Mean_{1^{st}\ phase\ before\ filtering}$	1.9926	2.2121	2.3818	2.4716	1.7898
$Mean_{1^{st}\ phase\ after\ filtering}$	1.2344	1.0484	1.2549	1.0953	0.64722
$Mean_{2^{nd}\ phase\ before\ filtering}$	2.1611	2.0794	2.4575	2.0818	1.779
$Mean_{2^{nd}\ phase\ after\ filtering}$	1.2755	1.2948	1.3664	1.3745	0.8963
$Mean_{3^{rd}\ phase\ before\ filtering}$	2.1328	2.1233	2.5764	2.4963	1.7762
$Mean_{3^{rd}\ phase\ after\ filtering}$	1.1927	1.2249	1.0953	1.3564	0.88409

Table 4.5 Time-averaged PLE signals for the CZ channel in the three phases of the protocol for filtered and unfiltered signals.

In Table 4.5 can be observed the averages of the different PLE values for the CZ channel over time during the protocol phases for filtered and unfiltered signals. It can be observed that the signals, during the unfiltered phase of the signal, have a much higher average. This is probably due to an artifact at low frequencies that makes the PLE higher. The nature of low frequency artifacts can be different, such as: variation in skin impedance, temperature variations, respiratory artifacts, movement artifacts, cardiac artifacts, ambient noise or an amplifier offset so an artifact common to all subjects and all recordings. The mean of the PLE signals, for unfiltered signals is 2.1675, while for filtered signals it is 1.0658. This implies that the average after filtering of signals is much lower than that with unfiltered signals. Experimentally, this implies totally different sounds during the acquisition with sound feedback. In fact, with the results obtained without filtering you could get noises all close to the brown noise or even with a greater scaling of the higher frequencies. This implies a much darker and less stimulating sound at the brain level.

	Subj 1	Subj 2	Subj 3	Subj 4	Subj 5
$SD_{1^{st}\ phase\ before\ filtering}$	0.06613	0.16314	0.13173	0.12555	0.12599
$SD_{1^{st}\ phase\ after\ filtering}$	0.091173	0.13953	0.11415	0.12382	0.11858
$SD_{2^{nd}\ phase\ before\ filtering}$	0.076772	0.11683	0.19881	0.12928	0.088608
$SD_{2^{nd}\ phase\ after\ filtering}$	0.10809	0.12747	0.077381	0.22802	0.13811
$SD_{3^{rd}\ phase\ before\ filtering}$	0.085802	0.13206	0.065764	0.14395	0.085893
$SD_{3^{rd}\ phase\ after\ filtering}$	0.21895	0.13704	0.12382	0.1562	0.092391

Table 4.6: Values of the standard deviations of PLE signals over time for the CZ channel in the three phases of the protocol for filtered and unfiltered signals.

In Table 4.6 it can be seen that the values of the standard deviations of the PLE signal for each subject. From the values given, there are no large variations in the values between the filtered and unfiltered signals as was the case for the averages. This implies that, despite the filtering, PLE values oscillate in a very similar range. The range of possible values for PLE is subjective, in fact, there are no similar or recurring standard deviation values between subjects and between different phases of the experiment.

Chapter 5: Conclusions

The NFB system implemented in ROS made it possible to achieve the primary objective, namely that of creating an auditory NFB that would work in real time by providing the subject with a sound proportional to his brain activity. The system is able to carry out real-time signal acquisition, recording, processing and elaboration through filtering and feature extraction techniques such as PSD and PLE. In addition, the sound generation proportional to the value of the PLE is correct as also indicated by the Fig. 4.17. Starting from the specifications of the system, it can be said that the choice of the four-second window is appropriate for carrying out the task. In fact, thanks to this window it is possible to calculate the PLE on the required frequency range. The choice of the exponential smoothing introduced with the proposed smoothing coefficient manages to perfectly capture the general trends of the PLE over time. The smoothing technique makes the signal less prone to noise, artifacts and sudden changes in the PSD but manages to capture the general trend over time. The scaling factor implemented through the power law turns out to be very effective for sound generation. In addition, the overlapping between the sound chunks allows for a smoother sound, without jumping and scratching, and therefore more pleasant. From the values extrapolated from the signals and from the visual inspection carried out, several conclusions can be drawn regarding the practice of NFB implemented and described in the previous chapters. In particular, the correlation indices between the PLE signals in the CZ channel and in the neighbouring channels increased dramatically as the filtering applied to the signal increased. It is possible to say that the signal deriving from CZ, in addition to being the cleanest, is able to capture the general trend of the PLE in the highlighted area very well. Complexity metrics have made it possible to investigate more about the trend of the PLE. In particular, it has been noted that the PLE is able to capture the general trend of the PSD well through a single index. The other metrics indicate trends for the individual frequency bands or relative trends between them but fail to capture the overall trend. The only index that was seen to be very similar to the PLE, was the SE. This index does not reflect a real meaning on the trend of the PSD, but only indicates the degree of complexity and disorder of it. The main problem with using the SE is that it is not possible to create a sound proportional to its trend over time since it covers a very different range of values from that of the PLE. The power law and therefore the scaling of white noise, in fact, could not be applied directly using the values of the SE but a calibration and subsequent scaling of the values would be necessary. For this reason, it is preferred to keep the PLE as a metric of complexity because, in addition to having optimal values for sound generation, it is able to capture the progress of the PSD. The values of the averages of the PLE signals calculated before and after the filtering of brain signals showed that the PLE values are much lower than the values used during feedback, causing a distortion of the noise. There is no difference between the range of values covered by the PLE of unfiltered and filtered signals. The standard deviation therefore remains a subject-dependent value. From the signals collected, from the topographic maps and from the considerations made, it emerges that there is no considerable variation in the PLE between the three different phases of the protocol. The averages of the PLE signals, like the standard deviations, do not appear to have changed during the phases. The linear signal trend of the PLE also remains uniform between subjects. Topographic maps do not show higher or lower occipital and temporal activity than average, indicating that there is no evident activation in certain bands. So, we can say that images and auditory feedback, applied as per protocol, had no effect of substantial change in the PLE. This result is positive because at this stage of the creation of the NFB there is no desire to perturb the brain system. In fact, at this stage, the only goal was to keep track of the progress of the PLE and to create a sound proportional to it. The fact that the brain waves remained unchanged in the three phases is a positive sign since it implies that the images do not arouse visual potentials and that the mere perception of external sounds does not disturb brain activity.

In these experiments, problems and limitations were highlighted that should be taken into account in subsequent work. First of all, it was noticed that the recorded signal had a low-frequency component that led to oscillations during recording. This is likely due to an inherent artifact of the EEG cap or power supply as the phenomenon occurred for each subject. The ultra-low frequency components present may have increased the PSD values in the Delta frequency band thus leading to higher PLE values. The actual finding of this problem was observed in the analysis with filtering in which a bandpass filter was applied which allowed to obtain much lower PLE values. To avoid this problem, we could proceed in two different ways. The first is to apply a real-time bandpass filtering through the implementation of digital filters, paying attention to the specifics of the task. The use of online digital filters could increase the computational cost of NFB leading to latencies in the tracking of neural activity and therefore to late sound generation. The second method starts from the hypothesis that we want to have a congruous value of PLE between the unfiltered and filtered signals. To do this, it could be proceeded with a PLE calibration phase for the individual subject and compare the PLE values derived from unfiltered signals with those derived from filtered signals. Once the average value of both signals has been obtained, you can proceed with the calculation of the difference between the two and enter the resulting value in the code as a shift from the actual values coming out of the fit on the PSD. Obviously, this technique would not allow to obtain precise values of the PLE, but it would allow to obtain similar results without increasing the computational complexity of the system. Another problem encountered during the experiments was eye movement, in fact, there was a high correlation between the values of the EOG signal and the recorded signals. In particular, this phenomenon was highlighted in the frontal area of the scalp of the subjects. From Table 4.1 it was possible to see that the introduction of images does not seem to have worsened the artifacts due to eye movement. In most cases, however, it has made it possible to reduce this artifact. Techniques such as ICA still remain prohibitive in such an environment given the amount of computation required to reduce the EOG signal from brain signals. In the future, deep learning techniques such as Recurrent Neural Networks (RNNs) or Convolutional Neural Networks (CNNs) could be developed. The idea could be to train neural networks for the recognition and subtraction of ocular artifacts from the EEG. A pre-trained model could be implemented in real time, before the PSD calculation phase. The model must be trained on EEG data with and without EOG artifacts to learn how to remove the EOG contribution correctly. A large amount of data would be required for training and the model should still be lightweight to allow filtering operations to be carried out in the shortest possible time. Identifying predictable and regular artifacts remains the primary limitation of this approach.

The NFB presented in this work does not represent a final version, but a preliminary phase that allows us to draw some useful conclusions for the future development of the project. The final NFB, in fact, will involve the perturbation of brain activity and not just the tracking of it. To do this, it will be necessary to create a system that keeps track of the subject's activity and that, instead of sending a sound proportional to it, sends a sound to try to modulate the subject's frequency spectrum. To do this, changes will have to be made to the system and protocol, as well as to investigate brain activity more. First of all, it would be necessary to investigate the performance of the PLE in response to auditory stimuli. This would make it possible to understand in which cases an actual auditory response occurs. Next, I would verify the existence of repercussions on the global brain activity of the auditory stimuli administered. This will allow, in addition to having a broader knowledge of brain behaviour in response to sounds, to be able to pick up the PLE signal in the most suitable area for the final goal. As far as experiments are concerned, some changes will have to be made with respect to the protocol already carried out. The future protocol should not have three separate phases, with three respective registrations, but a single registration should be carried out. At the beginning of the protocol there will be no images, but the white cross will be displayed in the centre. This phase could be used for the calibration of some parameters useful for the experiment. After the time frame set for the calibration phase, the images will be shown on the screen. This phase in future studies could be used to further investigate the effect of images on brain activity. If it is highlighted again that the images have no effect on brain activity, one of the two phases prior to the generation of sound could be eliminated, to reduce calibration times and reduce the length of the experiment. Finally, after the first two phases, we will proceed with the generation of sound for the perturbation of the brain system. This phase could be longer than the ten minutes proposed to be able to investigate the progress of the PLE in prolonged times. The sound heard can always be administered as variations of coloured noise or as melodies. Finally, the values of the proposed complexity metrics could be integrated into the PLE to have a final value that allows to capture more faithfully the actual trend of the content in frequency.

Bibliography

[1] Schnitzler A, Gross J. Normal and pathological oscillatory communication in the brain. Nat Rev Neurosci. 2005 Apr;6(4):285-96. doi: 10.1038/nrn1650. PMID: 15803160.

[2] Perez V, Duque A, Hidalgo V, Salvador A. EEG frequency bands in subjective cognitive decline: A systematic review of resting state studies. Biol Psychol. 2024 Sep; 191:108823. doi: 10.1016/j.biopsycho.2024.108823. Epub 2024 May 28. PMID: 38815895.

[3] Trambaiolli LR, Cassani R, Mehler DMA, Falk TH. Neurofeedback and the Aging Brain: A Systematic Review of Training Protocols for Dementia and Mild Cognitive Impairment. Front Aging Neurosci. 2021 Jun 9; 13:682683. doi: 10.3389/fnagi.2021.682683. PMID: 34177558; PMCID: PMC8221422.

[4] Li, X., Zhang, J., Li, XD. et al. Neurofeedback Training for Brain Functional Connectivity Improvement in Mild Cognitive Impairment. J. Med. Biol. Eng. 40, 484–495 (2020), doi: https://doi.org/10.1007/s40846-020-00531-w

[5] Moretti DV. Theta and alpha EEG frequency interplay in subjects with mild cognitive impairment: evidence from EEG, MRI, and SPECT brain modifications. Front Aging Neurosci. 2015 Mar 20; 7:31. doi: 10.3389/fnagi.2015.00031. PMID: 25926789; PMCID: PMC4396516.

[6] McBride JC, Zhao X, Munro NB, Smith CD, Jicha GA, Hively L, Broster LS, Schmitt FA, Kryscio RJ, Jiang Y. Spectral and complexity analysis of scalp EEG characteristics for mild cognitive impairment and early Alzheimer's disease. Comput Methods Programs Biomed. 2014 Apr;114(2):153-63. doi: 10.1016/j.cmpb.2014.01.019. Epub 2014 Feb 8. PMID: 24598317; PMCID: PMC4021716.

[7] van der Hiele K, Vein AA, Reijntjes RH, Westendorp RG, Bollen EL, van Buchem MA, van Dijk JG, Middelkoop HA. EEG correlates in the spectrum of cognitive decline. Clin Neurophysiol. 2007 Sep;118(9):1931-9. doi: 10.1016/j.clinph.2007.05.070. Epub 2007 Jun 28. PMID: 17604688.

[8] Hidasi Z, Czigler B, Salacz P, Csibri E, Molnár M. Changes of EEG spectra and coherence following performance in a cognitive task in Alzheimer's disease. Int J Psychophysiol. 2007 Sep;65(3):252-60. doi: 10.1016/j.ijpsycho.2007.05.002. Epub 2007 May 13. PMID: 17586077.

[9] Jeong J. EEG dynamics in patients with Alzheimer's disease. Clin Neurophysiol. 2004 Jul;115(7):1490-505. doi: 10.1016/j.clinph.2004.01.001. PMID: 15203050.

[10] Sitaram R, Ros T, Stoeckel L, Haller S, Scharnowski F, Lewis-Peacock J, Weiskopf N, Blefari ML, Rana M, Oblak E, Birbaumer N, Sulzer J. Closed-loop brain training: the science of neurofeedback. Nat Rev Neurosci. 2017 Feb;18(2):86-100. doi: 10.1038/nrn.2016.164. Epub 2016 Dec 22. Erratum in: Nat Rev Neurosci. 2019 May;20(5):314. doi: 10.1038/s41583-019-0161-1. PMID: 28003656.

[11] Sharon Niv, Clinical efficacy and potential mechanisms of neurofeedback, Personality and Individual Differences, Volume 54, Issue 6, 2013, Pages 676-686, ISSN 0191-8869, https://doi.org/10.1016/j.paid.2012.11.037.

[12] Hammond, D. C. (2007). What Is Neurofeedback? Journal of Neurotherapy, 10(4), 25–36. https://doi.org/10.1300/J184v10n04_04

[13] Marzbani H, Marateb HR, Mansourian M. Neurofeedback: A Comprehensive Review on System Design, Methodology and Clinical Applications. Basic Clin Neurosci. 2016 Apr;7(2):143-58. doi: 10.15412/J.BCN.03070208. PMID: 27303609; PMCID: PMC4892319.

[14] Deilami M, Jahandideh A, Kazemnejad Y, Fakour Y, Alipoor S, Rabiee F, Pournesaie GS, Heidari RN, Mosavi SA. The Effect of Neurofeedback Therapy on Reducing Symptoms Associated with Attention Deficit Hyperactivity Disorder: A Case Series Study. Basic Clin Neurosci. 2016 Apr;7(2):167-71. doi: 10.15412/J.BCN.03070211. PMID: 27303612; PMCID: PMC4892322.

[15] Heinrich H, Busch K, Studer P, Erbe K, Moll GH, Kratz O. EEG spectral analysis of attention in ADHD: implications for neurofeedback training? Front Hum Neurosci. 2014 Aug 21; 8:611. doi: 10.3389/fnhum.2014.00611. PMID: 25191248; PMCID: PMC4139738.

[16] Kamida A, Shimabayashi K, Oguri M, Takamori T, Ueda N, Koyanagi Y, Sannomiya N, Nagira H, Ikunishi S, Hattori Y, Sato K, Fukuda C, Hirooka Y, Maegaki Y. EEG Power Spectrum Analysis in Children with ADHD. Yonago Acta Med. 2016 Jun 29;59(2):169-73. PMID: 27493489; PMCID: PMC4973024.

[17] A. Zhang, B. Yang and L. Huang, "Feature Extraction of EEG Signals Using Power Spectral Entropy," 2008 International Conference on BioMedical Engineering and Informatics, Sanya, China, 2008, pp. 435-439, doi: 10.1109/BMEI.2008.254.

[18] Zilio F, Gomez-Pilar J, Chaudhary U, Fogel S, Fomina T, Synofzik M, Schöls L, Cao S, Zhang J, Huang Z, Birbaumer N, Northoff G. Altered brain dynamics index levels of arousal in complete locked-in syndrome. Commun Biol. 2023 Jul 20;6(1):757. doi: 10.1038/s42003-023-05109-1. PMID: 37474587; PMCID: PMC10359418.

[19] Başar E, Güntekin B. A review of brain oscillations in cognitive disorders and the role of neurotransmitters. Brain Res. 2008 Oct 15; 1235:172-93. doi: 10.1016/j.brainres.2008.06.103. Epub 2008 Jul 2. PMID: 18640103.

[20] Zilio F, Gomez-Pilar J, Cao S, Zhang J, Zang D, Qi Z, Tan J, Hiromi T, Wu X, Fogel S, Huang Z, Hohmann MR, Fomina T, Synofzik M, Grosse-Wentrup M, Owen AM, Northoff G. Are intrinsic neural timescales related to sensory processing? Evidence from abnormal behavioral states. Neuroimage. 2021 Feb 1; 226:117579. doi: 10.1016/j.neuroimage.2020.117579. Epub 2020 Nov 20. PMID: 33221441.

[21] Vernon DJ. Can neurofeedback training enhance performance? An evaluation of the evidence with implications for future research. Appl Psychophysiol Biofeedback. 2005 Dec;30(4):347-64. doi: 10.1007/s10484-005-8421-4. PMID: 16385423.
[22] Ros T, J Baars B, Lanius RA, Vuilleumier P. Tuning pathological brain oscillations with neurofeedback: a systems neuroscience framework. Front Hum Neurosci. 2014 Dec 18; 8:1008. doi: 10.3389/fnhum.2014.01008. PMID: 25566028; PMCID: PMC4270171.
[23] Kolb B, Whishaw IQ. Brain plasticity and behavior. Annu Rev Psychol. 1998; 49:43-64. doi: 10.1146/annurev.psych.49.1.43. PMID: 9496621.
[24] Omejc N, Rojc B, Battaglini PP, Marusic U. Review of the therapeutic neurofeedback method using electroencephalography: EEG Neurofeedback. Bosn J Basic Med Sci. 2019 Aug 20;19(3):213-220. doi: 10.17305/bjbms.2018.3785. PMID: 30465705; PMCID: PMC6716090.
[25] Enriquez-Geppert S, Huster RJ, Herrmann CS. EEG-Neurofeedback as a Tool to Modulate Cognition and Behavior: A Review Tutorial. Front Hum Neurosci. 2017 Feb 22; 11:51. doi: 10.3389/fnhum.2017.00051. PMID: 28275344; PMCID: PMC5319996.
[26] N. H. A. Hamid, N. Sulaiman, S. A. M. Aris, Z. H. Murat and M. N. Taib, "Evaluation of human stress using EEG Power Spectrum," 2010 6th International Colloquium on Signal Processing & its Applications, Malacca, Malaysia, 2010, pp. 1-4, doi: 10.1109/CSPA.2010.5545282.
[27] Klimesch W. EEG alpha and theta oscillations reflect cognitive and memory performance: a review and analysis. Brain Res Brain Res Rev. 1999 Apr;29(2-3):169-95. doi: 10.1016/s0165-0173(98)00056-3. PMID: 10209231.
[28] Takabatake K, Kunii N, Nakatomi H, Shimada S, Yanai K, Takasago M, Saito N. Musical Auditory Alpha Wave Neurofeedback: Validation and Cognitive Perspectives. Appl Psychophysiol Biofeedback. 2021 Dec;46(4):323-334. doi: 10.1007/s10484-021-09507-1. Epub 2021 Apr 30. PMID: 33929674; PMCID: PMC8553721.
[29] Clarke AR, Barry RJ, Karamacoska D, Johnstone SJ. The EEG Theta/Beta Ratio: A marker of Arousal or Cognitive Processing Capacity? Appl Psychophysiol Biofeedback. 2019 Jun;44(2):123-129. doi: 10.1007/s10484-018-09428-6. PMID: 30604100.
[30] Perrottelli A, Giordano GM, Brando F, Giuliani L, Pezzella P, Mucci A, Galderisi S. Unveiling the Associations between EEG Indices and Cognitive Deficits in Schizophrenia-Spectrum Disorders: A Systematic Review. Diagnostics (Basel). 2022 Sep 9;12(9):2193. doi: 10.3390/diagnostics12092193. PMID: 36140594; PMCID: PMC9498272.
[31] Başar E. Brain oscillations in neuropsychiatric disease. Dialogues Clin Neurosci. 2013 Sep;15(3):291-300. doi: 10.31887/DCNS.2013.15.3/ebasar. PMID: 24174901; PMCID: PMC3811101.

[32] Basar E, Basar-Eroglu C, Karakas S, Schürmann M. Oscillatory brain theory: a new trend in neuroscience. IEEE Eng Med Biol Mag. 1999 May-Jun;18(3):56-66. doi: 10.1109/51.765190. PMID: 10337564.

[33] Birbaumer N, Ramos Murguialday A, Weber C, Montoya P. Neurofeedback and brain-computer interface clinical applications. Int Rev Neurobiol. 2009; 86:107-17. doi: 10.1016/S0074-7742(09)86008-X. PMID: 19607994.

[34] Chaddad A, Wu Y, Kateb R, Bouridane A. Electroencephalography Signal Processing: A Comprehensive Review and Analysis of Methods and Techniques. Sensors (Basel). 2023 Jul 16;23(14):6434. doi: 10.3390/s23146434. PMID: 37514728; PMCID: PMC10385593.

[35] Klar P, Çatal Y, Langner R, Huang Z, Northoff G. Scale-free dynamics in the core-periphery topography and task alignment decline from conscious to unconscious states. Commun Biol. 2023 May 9;6(1):499. doi: 10.1038/s42003-023-04879-y. PMID: 37161021; PMCID: PMC10170069.

[36] Klar P, Çatal Y, Langner R, Huang Z, Northoff G. Scale-free dynamics of core-periphery topography. Hum Brain Mapp. 2023 Apr 1;44(5):1997-2017. doi: 10.1002/hbm.26187. Epub 2022 Dec 29. PMID: 36579661; PMCID: PMC9980897.

[37] Kozhushko NJ, Nagornova ZV, Evdokimov SA, Shemyakina NV, Ponomarev VA, Tereshchenko EP, Kropotov JD. Specificity of spontaneous EEG associated with different levels of cognitive and communicative dysfunctions in children. Int J Psychophysiol. 2018 Jun; 128:22-30. doi: 10.1016/j.ijpsycho.2018.03.013. Epub 2018 Mar 22. PMID: 29577946.

[38] Bucho T, Caetano G, Vourvopoulos A, Accoto F, Esteves I, I Badia SB, Rosa A, Figueiredo P. Comparison of Visual and Auditory Modalities for Upper-Alpha EEG-Neurofeedback. Annu Int Conf IEEE Eng Med Biol Soc. 2019 Jul; 2019:5960-5966. doi: 10.1109/EMBC.2019.8856671. PMID: 31947205.

[39] G. Beraldo, S. Tortora, E. Menegatti and L. Tonin, "ROS-Neuro: implementation of a closed-loop BMI based on motor imagery," 2020 IEEE International Conference on Systems, Man, and Cybernetics (SMC), Toronto, ON, Canada, 2020, pp. 2031-2037, doi: 10.1109/SMC42975.2020.9282968.

[40] Tonin Luca, Beraldo Gloria, Tortora Stefano, Menegatti Emanuele, ROS-Neuro: An Open-Source Platform for Neurorobotics, Frontiers in Neurorobotics, 16, 2022, doi: 10.3389/fnbot.2022.886050

[41] L. Tonin, G. Beraldo, S. Tortora, L. Tagliapietra, J. d. R. Millán and E. Menegatti, "ROS-Neuro: A common middleware for BMI and robotics. The acquisition and recorder packages," 2019 IEEE International Conference on Systems, Man and Cybernetics (SMC), Bari, Italy, 2019, pp. 2767-2772, doi: 10.1109/SMC.2019.8914364.

[42] Bachmann M, Lass J, Suhhova A, Hinrikus H. Spectral asymmetry and Higuchi's fractal dimension measures of depression electroencephalogram. Comput Math Methods Med. 2013; 2013:251638. doi: 10.1155/2013/251638. Epub 2013 Oct 22. PMID: 24232245; PMCID: PMC3819823.

[43] Hinrikus H, Suhhova A, Bachmann M, Aadamsoo K, Võhma U, Lass J, Tuulik V. Electroencephalographic spectral asymmetry index for detection of depression. Med Biol Eng Comput. 2009 Dec;47(12):1291-9. doi: 10.1007/s11517-009-0554-9. Epub 2009 Nov 13. PMID: 19911211.

[44] Wang Yao , Sokhadze Estate M. , El-Baz Ayman S. , Li Xiaoli , Sears Lonnie , Casanova Manuel F., Tasman Allan, Relative Power of Specific EEG Bands and Their Ratios during Neurofeedback Training in Children with Autism Spectrum Disorder, Frontiers in Human Neuroscience, 9, 2016, doi:10.3389/fnhum.2015.00723

[45] Hillard B, El-Baz AS, Sears L, Tasman A, Sokhadze EM. Neurofeedback Training Aimed to Improve Focused Attention and Alertness in Children With ADHD: A Study of Relative Power of EEG Rhythms Using Custom-Made Software Application. Clinical EEG and Neuroscience. 2013;44(3):193-202. doi:10.1177/1550059412458262

[46] Jwo, Dah-Jing & Chang, Wei-Yeh & Wu, I-Hua. (2021). Windowing Techniques, the Welch Method for Improvement of Power Spectrum Estimation. Computers, Materials & Continua. 67. 3983-4003, doi:10.32604/cmc.2021.014752.